論文 / 著書情報
Article / Book Information

題目(和文)	全固体電池における電極/硫化物系固体電解質の界面反応
Title(English)	Interfacial reactions at electrode/sulfide-based solid electrolyte in all-solid-state batteries
著者(和文)	佐久間将実
Author(English)	Masamitsu Sakuma
出典(和文)	学位:博士(工学), 学位授与機関:東京工業大学, 報告番号:甲第10031号, 授与年月日:2015年12月31日, 学位の種別:課程博士, 審査員:菅野 了次,大坂 武男,北村 房男　,中村 二朗,平山 雅章
Citation(English)	Degree:Doctor (Engineering), Conferring organization: Tokyo Institute of Technology, Report number:甲第10031号, Conferred date:2015/12/31, Degree Type:Course doctor, Examiner:,,,,
学位種別(和文)	博士論文
Type(English)	Doctoral Thesis

Interfacial reactions at electrode/sulfide-based solid electrolyte in all-solid-state batteries

（全固体電池における電極/硫化物系固体電解質の界面反応）

Masamitsu SAKUMA

Dissertation

Submitted to the Department of Electronic Chemistry
Interdisciplinary Graduate School of Science and Engineering
Tokyo Institute of Technology
In Partial Fulfillment of the Requirement for the Degree of

Doctor of Engineering

Tokyo Institute of Technology
December 2015

Table of Contents

CHAPTER 1

Introduction

1.1 Development of lithium-ion battery

As the issue of global warming increases in severity, technological development about energy and the environment has become more important. The search for energy sources to provide a comfort lifestyle has taken place since the beginning of the energy sources used, included fossil fuel, oil, nuclear energy, solar energy. A search of more efficient, clean and safe energy sources was taken from beginning of industrialization. Currently, as the engine car is a major user of fossil (oil), consuming about 1/3 of the annual total energy demand, concern over global warming and air pollution has become evident [1-1]. It is necessary to grow out of oil-dependent economy and to reduce the harmful effects on the environment. This causes the trend to develop the new products with the environment-friendly strategy. As a recent trend in the battery industry, the lithium-ion battery, and fuel cell technology have been acclaimed as advanced power sources, gradually replacing several versions of conventional systems such as the lead acid and nickel cadmium batteries [1-2]. Figure 1-1 shows the secondary battery sales (a) by value and (b) by volume. Battery Association of Japan started the sales for the secondary battery in 1986 [1-2], since than the sales continue to increase until 2008. It has been stabilized in the past few years. Similar trends have been observed even for sales of lithium ion battery. On the other hand, Fig.1-2 shows the secondary battery sale by value in the world market [1-3]. This figure shows that over all world demand for the secondary battery sales are still growing. Lithium-ion battery sales trend observed to be same and it occupied the highest share of the secondary batteries market. The sales of lithium-ion battery

continues increasing in Japan since the introduction of lithium ion battery, while the sales of other battery system either remained constant or decreased. Lithium-ion battery with the high energy density leads the market in miniature batteries. It is a compact and has longer life more than 500 charge/discharge cycles [1-4]. Since lithium-ion battery has been invented by a Japanese company in 1991, it has attracted much attention both of consumers and companies because of its high performance, high growth potential, and rapid increase in production. Lithium-ion batteries are the promising candidates for the next generation secondary batteries, because of the success of lithium-ion battery technology in the portable electronics market. However, it is necessary of further improvement. A key factor in designing electric or plug-in hybrid vehicles and energy storage devices for wind or solar power generation is the development of battery technologies that allow higher energy and power densities with suitable margins of safety. Although large-size lithium-ion batteries have many advantages over other types of secondary batteries, they are not sufficient as commercial scale. It is difficult to resolve the issues related to processing and safety at commercial scale [1-5]. The cause of the safety issues is due to the liquid electrolyte, for which organic liquid solvents such as PC, EC, DEC, DMC are utilized. Table 1 shows the boiling point, flash point, and ignition point of typical organic liquid electrolyte [1-6]. The flash points of the organic solvents are lower than 200°C, which temperature easily rises under severe use environment or at the short circuit in lithium ion battery [1-7]. There is possibility of leakage, fire, and burst in the batteries with liquid electrolyte under these circumstances [1-8].

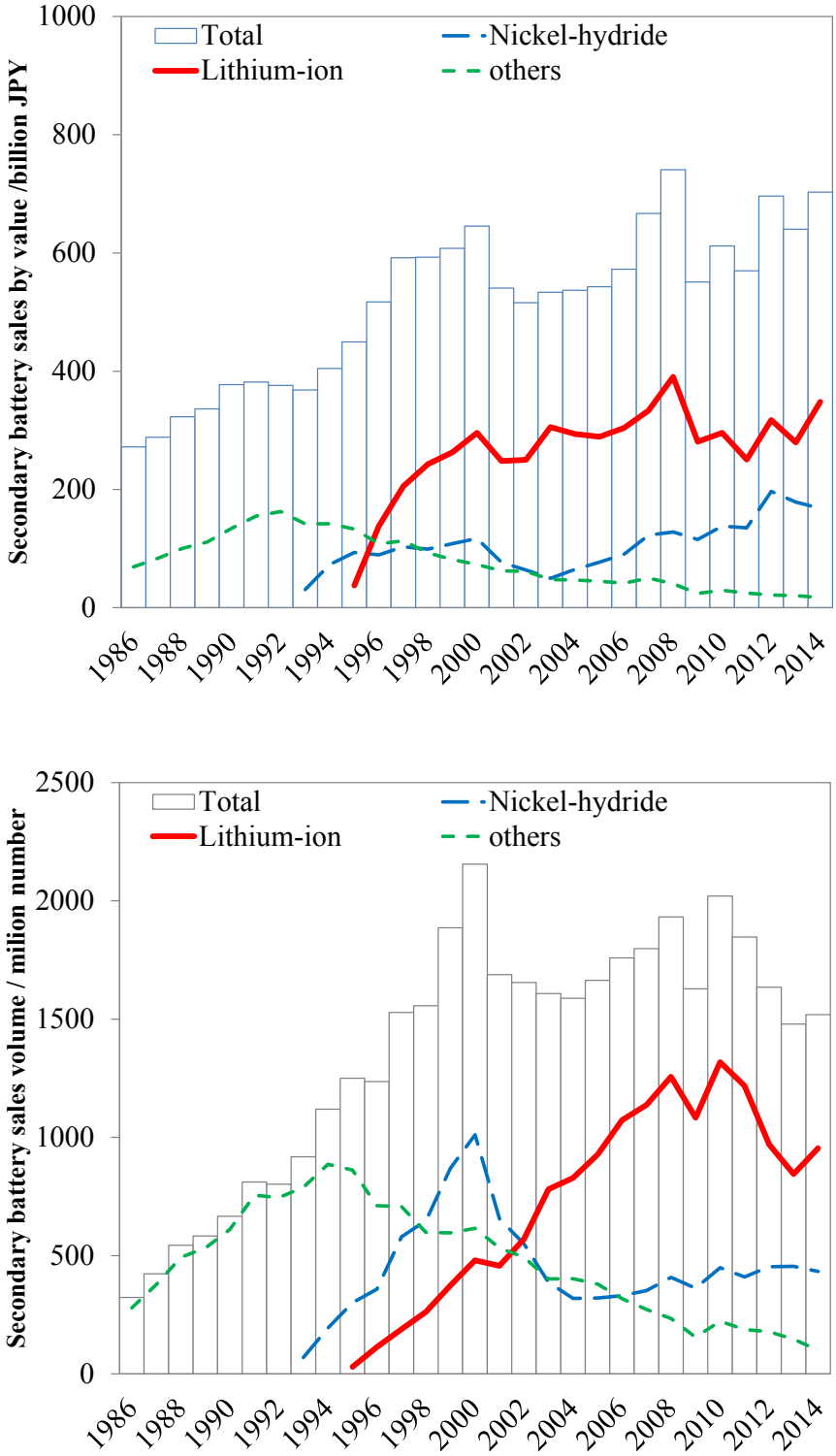

Figure 1-1 The secondary battery sales by (a) value and by (b) volume since the statistics for the secondary battery sales.

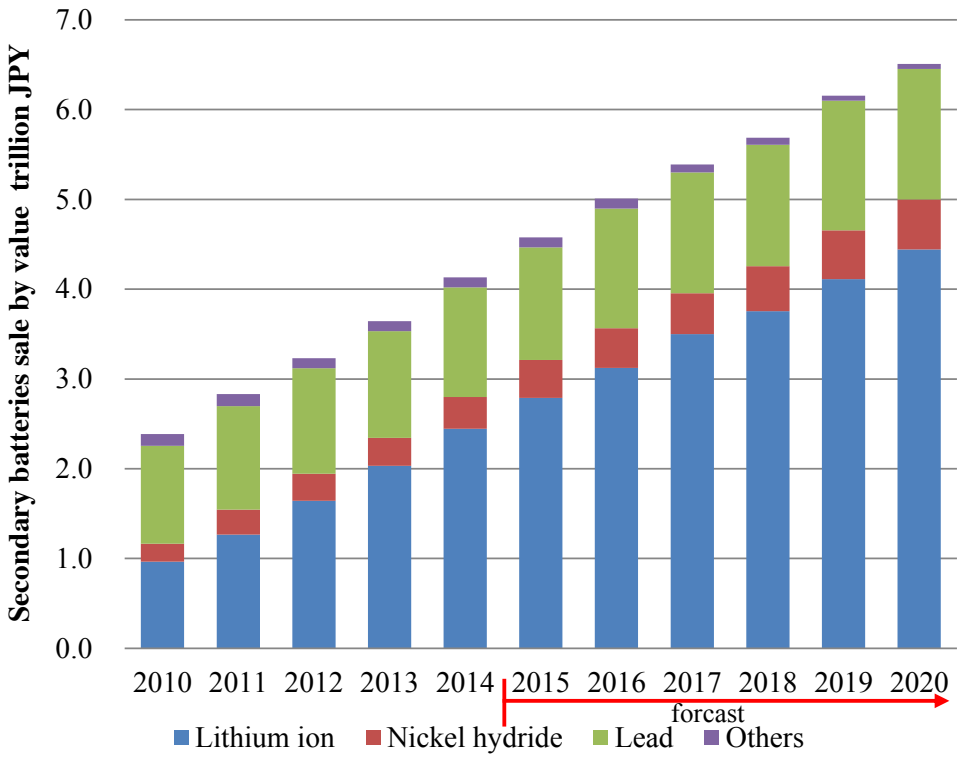

Figure 1-2 The secondary battery sales by value in the world market

(I cannot see the y-axis labels in these diagrams)

Table 1-1 The boiling point, flash point, and ignition point in typical organic liquid electrolyte

Organic solvent	Boiling point *t* / ℃	Flash point *t* / ℃	Ignition point *t* / ℃
Methyl-THF	80	-11	270
Diethyl ether	34	-40	160
Di-isoamyl ether	173	41	-
Di-isopropyl ether	68	-12	443
Dibutyl ether	142	25	194
Ethylmethyl ether	11	-37	190
Dimethyl ether	-24	-41	-
Propylene carbonate(PC)	243	160	-
Ethylene carbonate(EC)	240	132	-
Diethyl carbonate(DEC)	127	31	-
Ethylmethyl carbonate(EMC)	107	24	-
Dimethyl carbonate(DMC)	90	18	-

1.2 Importance of safety for lithium battery

Lithium-ion batteries may cause premature failure if subjected to conditions for which they are never designed [1-9, 10, 11, 12, 13]. Any misuse, including overcharging, external short-circuiting or crushing, could trigger self-heating reactions, which may lead to explosion. Lithium-ion batteries must pass some safety tests before they can be certified for use by consumers. The safety tests are included electrical tests such as external short circuit, mechanical tests such as nail penetration, crushing, dropping to the ground, and environmental tests such as heating in a microwave oven, throwing into a hot liquid, and leak tests in a vacuum. Some techniques have been developed to improve safety. They include use of safety vents [1-14], shutdown separators [1-15], more oxidation-tolerant or less flammable electrolyte constituents [1-16], and redox shuttle mechanisms [1-17]. Although many safety countermeasures prevent the lithium-ion batteries to have dangerous accidents under sever circumstance, it is difficult to eliminate those issues. However it is possible to change fundamental system of lithium-ion batteries for example change the liquid electrolyte system. The next generation for the new battery system will be the devices for using the other electrolytes with nonflammable materials instead of the organic flammable liquid electrolyte. Many researchers have reported the improvement of the safety for lithium-ion battery with gel-polymer electrolyte, ionic liquids electrolyte, and solid electrolyte. The safety of gel polymer electrolyte is almost same as that of liquid electrolyte due to the dissolving the polymerization products into liquid electrolyte, though the decomposition temperature of gel polymer electrolyte is higher than that of organic liquid electrolyte [1-18, 19]. Ionic liquids also have been reported actively as new electrolyte [1-20, 21]. Ionic liquid electrolyte is a salt composed of cation and anion, and it has many suitable properties required for better electrolyte of energy storage devices, such as non-flammability, and thermal stability [1-22, 23]. However, transport number is not enough for practical use, and ionic conductivity and activation energy with high-rate is not good at lower temperature [1-24, 25]. The organic liquid

electrolytes, gel polymer electrolytes, and ionic liquid electrolytes are not enough to attain the comprehensive battery performances for thermal, electrochemical, and electrical properties.

1.3 Which is better electrolyte – genuine solid polymer and ceramic solid material?

Characteristic of the solid electrolytes is to have an excellent safety [1-26]. The genuine solid polymer electrolyte and the ceramic solid electrolyte are being studied as the electrolyte of the all solid-state lithium batteries [1-27, 28]. Conventional solid polymer electrolytes used in the all solid-state lithium secondary batteries are poly (ethylene) oxide (PEO) and its derivatives [1-29, 30, 31, 32]. Most of polyether-based polymer electrolytes have low glass transition temperature [1-30]. In addition, solid polymer electrolytes are flexible at room temperature and can easily form thin film [1-33]. However, the solid polymer electrolyte is decomposed over 4V [*vs* Li/Li^+], and has the lower ionic conductivity at room temperature and the low lithium-ion transport number (t=0.3-0.6) [1-34]. On the other hand, safety improvement can be expected by replacing inflammable liquid electrolytes to non-flammable ceramic solid electrolytes. Batteries with ceramic solid electrolytes show good cycle performance, because the side reactions caused by the decomposition of solid electrolyte [1-35, 36, 37]. Ceramic solid electrolyte is stabilized thermodynamically up to 600°C and electrochemically up to 10 V *vs* Li/Li^+. Ceramic solid electrolyte is characterized by excellent thermal stability, electrochemical stability, and transport number. Ceramic solid electrolyte is the most suitable material for the ultimate all solid-state lithium secondary battery. In this study, sulfide-based solid electrolyte as ceramic solid electrolyte was used to study for lithium secondary batteries with high energy-density and high safety for practical application. (Repetition of words like Ceramic solid electrolyte)

1.4 Solid-State Ionics

Most solids, glasses, and alumina ceramics, are generally electrical insulation. However, class of solid called solid electrolytes can conduct electric current by ionic moving as well as electrolyte solutions. Ion conductivity is considerably different from electronic conductivity because the former conducts electric charges simultaneously with mass transport. Therefore, a chemical change can be connected to an electric phenomenon or action by applying solid electrolytes to batteries. In the field of solid state ionics, there are ionic crystals, organic polymer crystals, morphologies including single crystals, sintered ceramics, composites, thin film, and amorphous glass [1-38]. The solid materials with high ionic diffusion were found through the process of various materials design.

1.5 Comparison of crystalline and glassy lithium ionic conductor

Glassy materials and crystalline are classified as important ionic conductors. The difference between glassy ionic conductors and crystalline ionic conductors is as follows: the conductivity of glassy ionic conductors was improved the ionic mobility by deforming structure, and the conductivity of crystalline ionic conductors was improved by configuration suitable structure for high ionic diffusion. For silver ionic conductors, both glassy and crystalline ionic conductors show high ion conductivity (10^{-1}–10^{-2} Scm^{-1}) for AgI-Ag_2MoO_4 [1-39] and $RbAg_4I_5$ [1-40], respectively. However, the search of glassy materials is performed for lithium ionic conductors widely. Table 1-2 shows a typical example of glassy lithium ionic conductors.

Both sulfide and oxide glasses are generally considered as glassy ionic conductors. Oxide glasses are composed of network formers (SiO_2, GeO_2, and P_2O_5, etc) and network modifier (Li_2O). The increase of Li_2O, which is a network modifier, improves the conductivities of oxide glasses. However, the addition of the modifier to a given network causes the break of oxygen bridges. As the number of non-bridging oxygen atom increases, ionic conductivity decreases. Therefore, the conductivities of

oxide glasses are not so high (~ 10^{-6} Scm^{-1}) at room temperature.

Study of the sulfide glasses has a greater impact as replacing larger and more polarizable sulfur for oxygen. Li_2S-SiS_2 [1-41] glass systems are better ionic conductor and offer good thermal stability. In addition, they are easy to synthesize. Li_2S-SiS_2-Li_3PO_4 [1-42] glass system exhibits high ionic conductivity (> 10^{-3} Scm^{-1}) and high electrochemical stability. It is also reported that all solid-state batteries with sulfide glasses as electrolytes showed good charge-discharge performance [1-46, 47, 48].

Table 1-2 Conductivity of glassy lithium ionic conductors.

Compound	Conductivity at r.t. (σ / Scm^{-1})	Reference	
Li_2S-SiS_2	1.5 x 10^{-4}	Kennedy *et al*. (1987)	[1-41]
Li_2S-SiS_2-LiI	1.3 x 10^{-3}	Kennedy *et al*. (1987)	[1-41]
Li_2S-SiS_2-Li_3PO_4	1.8 x 10^{-3}	Kondo *et al*. (1992)	[1-42]
Li_2S-SiS_2-Li_4SiO_4	2.0 x 10^{-3}	Hirai *et al*. (1995)	[1-44]
Li_3PO_4-Li_4SiO_4	~10^{-6}	Miyauchi *et al*. (1982)	[1-44]
Li_3BO_4-Li_4SiO_4	~10^{-6}	Tatsumisago *et al*. (1987)	[1-45]

Although lithium ionic conductors in sulfide glass system have excellent properties, few studies of sulfide crystalline system have been reported. This is because crystalline materials are believed to be difficult to offer high ionic conductivity. However, the conductivity of crystalline material, $RbAg_4I_5$ (0.28 Scm^{-1}) [1-40], shows higher than that of AgI-Ag_2MoO_4 glass (2.1 x 10^{-2} Scm^{-1}) [1-39] by one order of magnitude. Since crystalline materials would have a close relationship between the conductivities and the structures, they might have higher conductivities than the corresponding glasses if their crystal structures are designed for high ionic conductivity. In addition, crystalline materials are also thermally stabilized, while glass materials have the glass transition temperature and the crystallization temperature under melting temperature. Only a few materials have been investigated previously in the crystalline sulfides family. Table 1-3 shows a typical example of crystalline sulfide and oxide

lithium ionic conductors; Li_3PS_4 [1-49], Li_2SiS_3 [1-50], and Li_4SiS_4 [1-50] were reported to have conductivities of $10^{-6} – 10^{-8}$ Scm^{-1} at room temperature. However, the conductivities of sulfides crystalline materials are higher than those of corresponding oxides crystalline materials as well as glassy materials.

Table 1-3 Conductivity of crystalline sulfide and oxide lithium ionic conductors.

Compound	Conductivity at r.t. (σ / Scm^{-1})	Reference	
Li_3PS_4	3.0 x 10^{-7}	Tachez *et al*. (1984)	[1-49]
Li_2SiS_3	2.0 x 10^{-6}	Huggins *et al*. (1989)	[1-50]
Li_4SiS_4	5.0 x 10^{-8}	Huggins *et al*. (1989)	[1-50]
Li_3PO_4	~10^{-18}	Wang *et al*. (1995)	[1-51]
Li_4GeO_4	~10^{-13}	Gratzer *et al*. (1971)	[1-52]
Li_4SiO_4	~10^{-11}	Gratzer *et al*. (1971)	[1-52]

1.6 Crystalline lithium ionic conductor

Table 1-4 shows a typical example of crystalline lithium ionic conductors.

- *LiI*

LiI is the first solid electrolyte, which was practically used in 1972 for Li/I batteries of heart pacemakers. This type of battery has high reliability because no internal short circuit occurs easily with automated formation of electrolyte between the anode and cathode. However, the use of electrolyte for all solid-state batteries is limited, because the conductivity of LiI is extremely low (~10^{-7} Scm^{-1}) at room temperature [1-53].

- *Li_3N*

Li_3N doped H is one of crystalline materials with high lithium ionic conductivity (~10^{-3} Scm^{-1}) [1-54]. The structure of Li_3N belong to the hexagonal and a layer structure [1-62], in which the layer of Li $(2)_2N$ and Li (1) are alternatively piled in the c axis direction (Fig. 1.3(a)). Lithium ionic conduction would mainly

take place along interlayer of Li (1). Since Li_3N decompose at low decomposition potential (0.445 V), which limits the use of electrolyte as a practical solid electrolyte in batteries [1-63]. Various Li_3N-derivative phases have been synthesized to improve decomposition potential.

- *Li-β-alumina*

Li-β-alumina could be synthesized by the Li ion-exchange method from Na-β-alumina. Both Li-β-alumina and Na-β-alumina is the similar structure [1-55]. The structure is a layered structure [1-64] in which densely packed blocks with spinel-like structure, alternate with open "conduction plane" containing the mobile Li^+ ions (Fig. 1.3(b)). Na-β-alumina is higher conductivity than by Li-β-alumina two orders of magnitude at room temperature. Na-β-alumina would be the most important solid electrolyte not only because it is practically useful in Na/S batteries, but also because it is expected electrolyte for large-scale batteries.

- *Li_2CdCl_4*

For halides, lithium chlorides [Li_2MCl_4 (M=Cod, Mg, Man, and V)] [1-56] have the inverse spinal structure, in which a half of the lithium ions is tetrahedral surrounded by chloride ions, and the remaining half, together with the M^{2+} ions, are distributed statistically over the octahedral sites. The spinal structure with the general formula, AB_2X_4, has cubic close packed X ions with A and B ions in tetrahedral and octahedral interstices, respectively (Fig. 1.3(c)).

- *$La_{0.5}Li_{0.5}TiO_3$*

The parasite given by the general formula, ABO_3 (A: alkaline metal, alkaline earth metal, and rare earth element, B: transition metal) has three-dimensional structure, and is also regarded as a framework structure with corner-sharing BO_6 octahedral and with A in twelve-coordinate interstices (Fig.

1.3(d)). This structure is stable and high ion conductivity because they have many vacancies of the *A* sites which would arise from the displacement of Li^+ ion. The lithium-containing parasite ($La_{2/3-x}Li_{3x}TiO_3$ [1-57]) system exhibits high conductivities (10^{-5} – 10^{-3} Scm^{-1}) because of the migration of Li^+ ion through the vacancies.

- *LISICON*

There exists the material family called LISICON (Lithium Supersonic Conductor) as the lithium ionic conductors. A wide variety of lithium ionic conductors have been synthesized based on the LISICON [$Li_{14}Zn(GeO_4)_4$] [1-53] system. The structure is related to the γ-Li_3PO_4 type [1-65] (Fig. 1.3(e)), and is formed by GeO_4, ZnO_4, PO_4, VO_4 tetrahedral or LiO_6 octahedral. A wide range of solid solutions were formed by univalent substitutions introduced interstitial lithium ions or lithium vacancies, and led to high ionic conductivities at higher temperatures.

A formation of solid solution is usually applied for performance improvement. The following two simple solid solution mechanisms are proposed:

1. *Substitution solid solutions:*

   The directly introduced atom or ion replaces an atom or ion of the same charge in the parent structure.

2. *Interstitial solid solutions:*

   The introduced species occupy a site, in which is normally empty, and no ions or atoms are left out.

Based on two basic types above, a variety of more complex solid solution mechanisms may be derived by having both substitution and interstitial formation together and by introducing ions of different charge in the host structure.

In fact, most solid solutions also have much more complex mechanisms. In univalent solid solution, ions are substituted by other ions of different charge, which causes consequently additional changes, creation of vacancies or interstitials (ionic compensation), electrons or holes (electronic compensation) to preserve electro neutrality. Figure 1-4 shows four types of action substitution for ionic compensation. A similar substitution is possible for anion but is not considered because anion substitution rarely occurs in solid solutions.

Among the LISICON family, the partial substitutions of higher valence Al^{3+} for Li^{+} in Li_4SiO_4 would introduce lithium vacancies, and the solid solution with the general formula, $Li_{4-3x}Al_xSiO_4$ [1-66] was obtained (Fig. 1-4(a)). In contrast, the extra lithium ions created by partial substitutions of lower valence Si^{4+} for P^{5+} in Li_3PO_4 would introduce interstitial lithium ions, and the solid solution with the general formula, $Li_{3+x}P_{1-x}Si_xO_4$ [1-60] was obtained (Fig. 1.4(d)). It is possible to design the structure, which is more suitable for the ionic conduction based on these substitutions.

Table 1-4 Conductivity of crystalline lithium ionic conductors.

Compound	Conductivity at r.t. (σ / Scm^{-1})	Reference	
LiI	5.5×10^{-7}	Schlaikjer *et al*. (1973)	[1-53]
Li_3N	1.0×10^{-3}	Lapp *et al*. (1983)	[1-54]
Li-β-alumina	1.3×10^{-4}	Whittingham *et al*. (1972)	[1-55]
Li_2CdCl_4	1.1×10^{-6}	Kanno *et al*. (1988)	[1-56]
$La_{0.5}Li_{0.5}TiO_3$	1.0×10^{-3}	Inaguma *et al*. (1994)	[1-57]
LISICON [$Li_{14}Zn(GeO_4)_4$]	6.0×10^{-7}	Hong *et al*. (1978)	[1-58]
$0.6Li_4GeO_4$–$0.4Li_3VO_4$	3.0×10^{-5}	West *et al*. (1980)	[1-59]
$0.5Li_3PO_4$–$0.5Li_4SiO_4$	4.0×10^{-6}	Hu *et al*. (1977)	[1-60]
$0.4Li_4SiO_4$–$0.6Li_3VO_4$	1.7×10^{-5}	Kuwano *et al*. (1981)	[1-61]

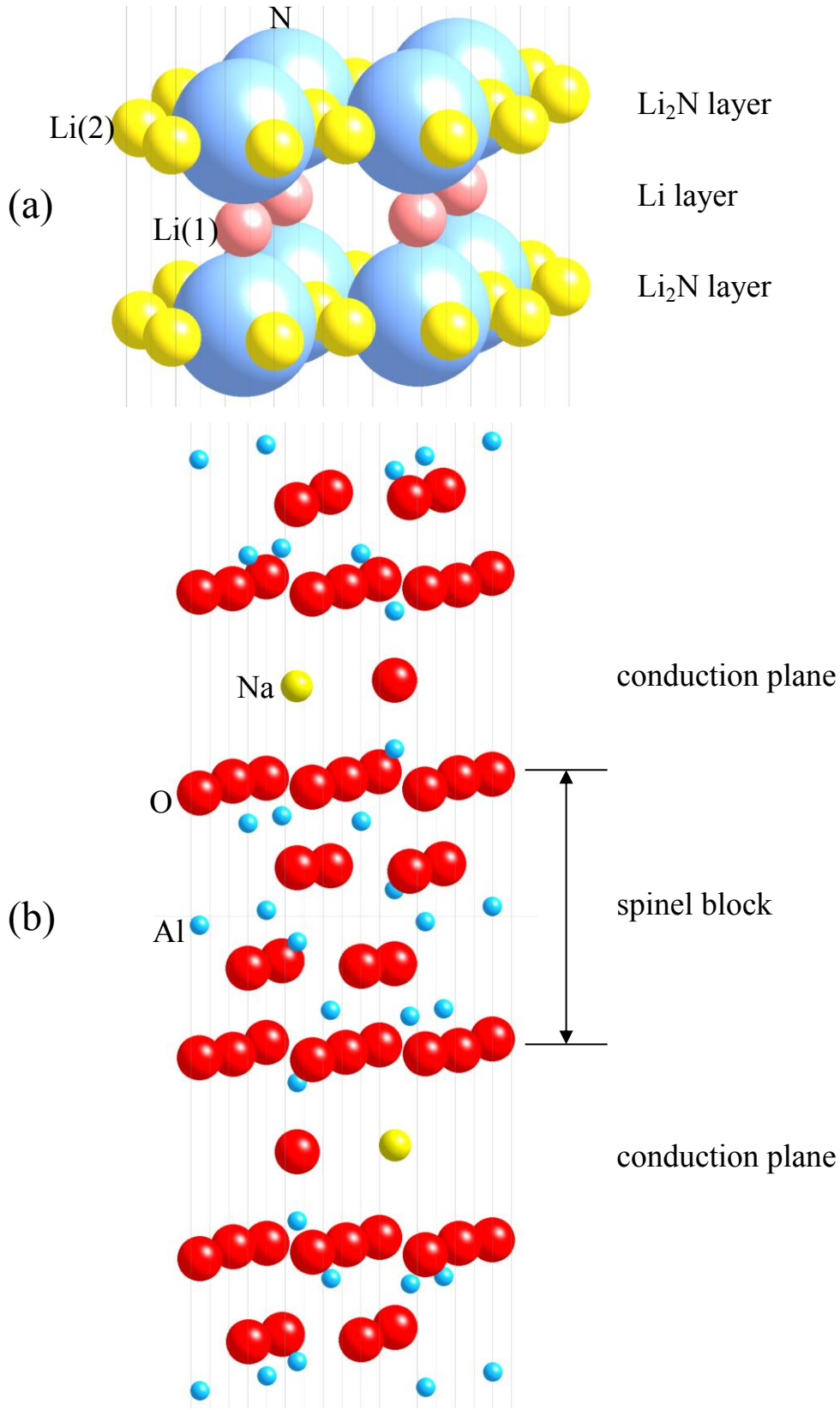

Figure 1-2 Structure of Li_3N (a), and β-Alumina (b).

(c)

(d)

(e)

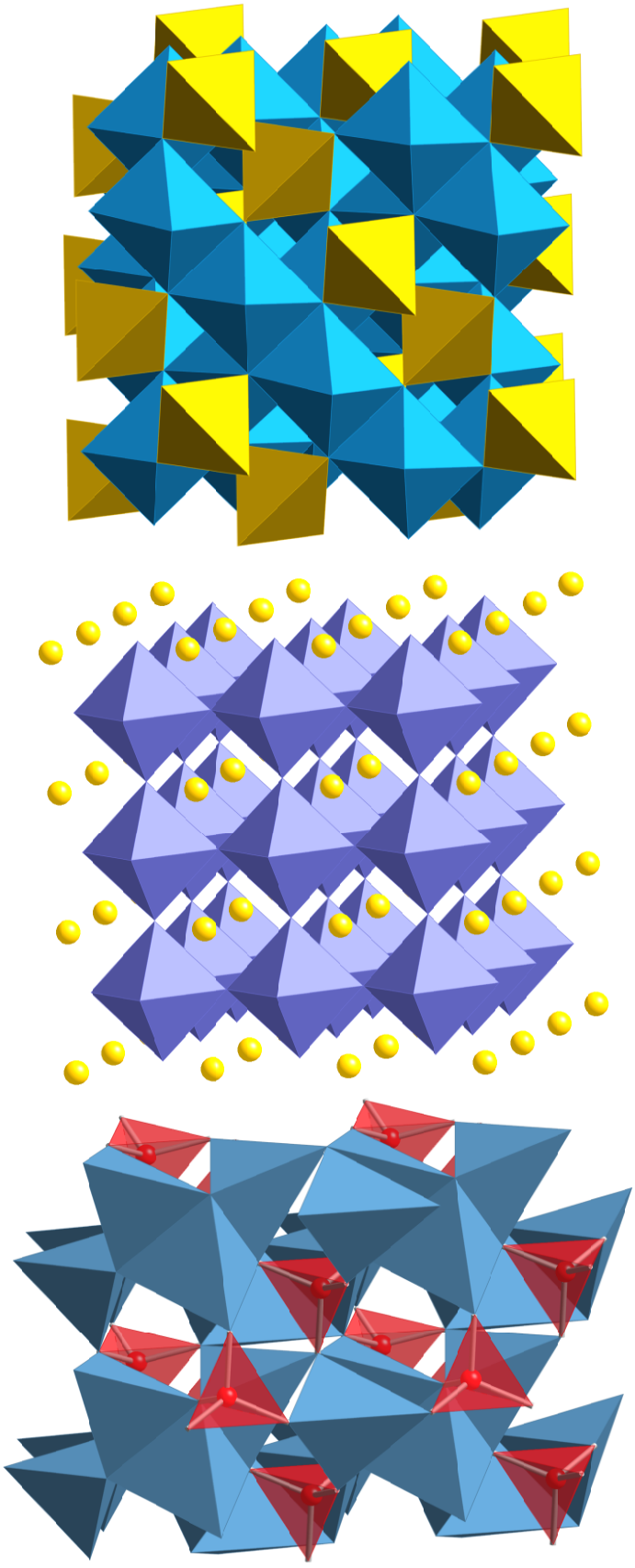

Figure 1-3 Crystal structures: spinel type (c), perovskite type (d), and γ-Li_3PO_4 type (e).

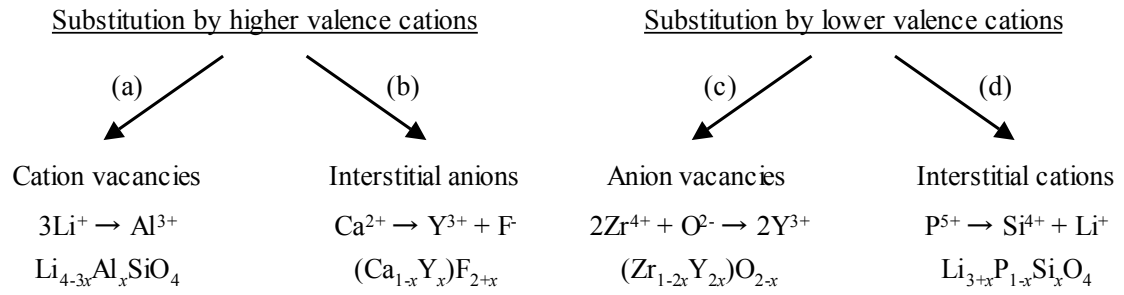

Figure 1-4 Solid solution formation by substitution of aliovalent cations.

1.7 Conduction mechanism

The concept of the defects and interstitial atoms, which provided a base in the field of solid state ionic, was proposed by Jeff [1-67] in 1923 immediately after discovery of α-Age. The regular lattice points in an ideal crystal are completely occupied by the atoms without disordered, and there are no interstitial atoms at the same time (Fig. 1-5 (a)). However, in real crystals, there exist both lattice points which are not occupied by atoms (Fig. 1-5 (b)) and which are not located at the regular lattice points (Fig. 1-5 (c)). The former is called a vacancy, and the latter is called an interstitial atom. Figure 1-5 (b) and 1-5 (c) shows imperfect nature of atomic arrangements, which is defined as point defects. Some properties of crystals, ionic diffusion coefficient, ionic conductivity, are drastically influenced by a low amount of point defects. Point defects have played a very important role in crystals. The concept of point defects was inherited to Frenkel [1-68], Schottky [1-69], and Wagner [1-70].

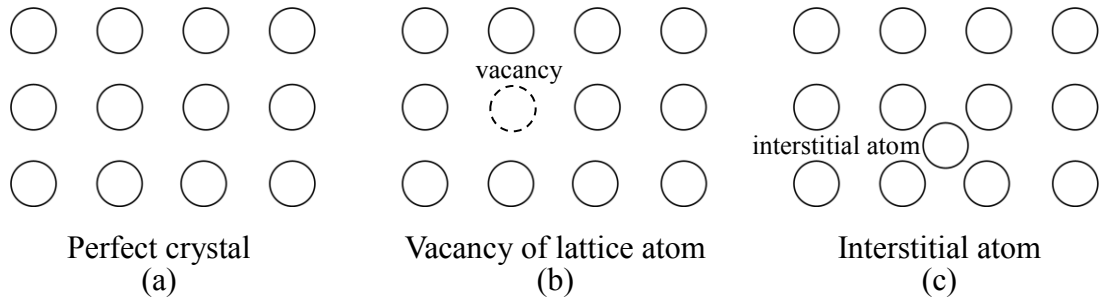

Figure 1-5 Perfect crystal (a), and crystals with point defects (b) and (c).

The thermodynamic theory of ionic conduction was established in the 1940's. The following two mechanisms may be regarded as point defects.

a) Schottky defect:

A stoichiometric defect is a pair of vacant sites, an anion vacancy and a cation vacancy (Fig. 1-6 (a)). There should be two extra atoms at the surface of the crystal for each defect to compensate for the vacancies. The numbers of anion and cation vacancies is equal in order to preserve local electroneutrality.

b) Frenkel defect:

This defect is formed a cation displaced in interstitial site and vacancy (Fig. 1-6 (b)). The vacancy and interstitial atom are oppositely charged, and attract each other to form pair.

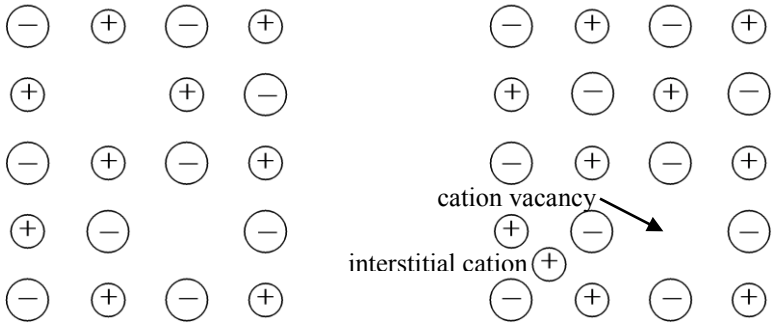

Schottky defect (a) Frenkel defect (b)

Figure 1-6 Types of point defect in ionic crystals.

Since the 1950's, the development of new materials based on these theoretical basis has been a key subject in this field. Copper ionic conductor, $Rb_4Cu_{16}I_7Cl_{13}$ [1-71, 72], discovered in the 1980's, is the highest ionic conductive solid, 0.34 Scm^{-1} at room temperature. From the discovery of classical material, α-AgI, to the success of stabilization of the highly conductive α-form at ambient temperatures, the research had been carried out for decades. The crystalline materials which have higher conductivity than $Rb_4Cu_{16}I_7Cl_{13}$ have not been discovered yet.

1.8 Materials design concept

Ionic conductors are intensively studied for their behaviors and structures as academic interest. Ionic conductors exhibit high ionic diffusion in one of their ionic sublattices at temperatures not higher than melting point of the ionic conductors [1-73]. It is of great interest to understand their fast ionic transport in solid materials, which is widely recognized, while it is still a relatively rare phenomenon [1-74]. The materials design concepts for high ionic conductor are as follows:

(I) Stabilizing the high conductive phase known until now at lower temperature by the partial substitutions of various cations and anions.

(II) Selection of material system which is composed by suitable framework structure for ionic conduction.

According to the concept (I), a result that many researchers studied to stabilize the structure of α-AgI near the room temperature. $Rb_4Cu_{16}I_7Cl_{13}$ [1-71, 72] and $RbAg_4I_5$ [1-75, 76], which have higher ionic conductivities than any copper and silver, were found. On the other hand, according to the concept(II), the lithium chloride spinel (Li_2MCl_4) [1-77] and oxides such as NASICON ($Na_{1+x}Zr_2P_{3-x}Si_xO_{12}$) [1-19] and LISICON [$Li_{14}Zn(GeO_4)_4$] [1-58] were discovered. The concept (I) is usually applicable to copper or silver conducting phase, the concept (II) is alkaline ionic conductors such as lithium and sodium. If the framework structure of host material is decided, the techniques of the usual solid state chemistry may be improved dramatically the conductivity. These are based on the following three structural criteria [1-73].

(a) Introduction of vacancies or interstitial ions by aliovalent substetutions in the lattice.

(b) Improvement of bottleneck for conductive path by replacing ions with different ionic radii.

(c) Selection of highly polarizable mobile ions and anion sublattices.

Many materials have been synthesized based on the above criteria of (a) and (b). The LISICON [1-58] system is a typical example of materials designed using the above criteria. A wide variety of materials with the same type of framework structure have been synthesized; a wide range of solid solutions formed by aliovalent substitutions introduced interstitial lithium ions or vacancies improve high ionic

conductivities at high temperatures [1-73]. However, the conductivity at room temperature (~10^{-6} Scm^{-1} for $Li_{3.6}Si_{0.6}P_{0.4}O_4$ [1-60, 74]) are still lower than those of copper and silver ionic conductors.

1.9 Materials system selection

The materials design of crystalline ionic conductors is based on certain structural criteria [1-73] to improve ionic conductivity. It is also important to consider the structural criteria (c) in the above section, when the search of new material family is carried out. Firstly, the replacement oxygen of the LISICON to sulfur is selected in order to improve ionic conductivity. Sulfides have many advantages over oxides for constructing ionic conductors; larger ionic radii, high polarizable character of sulfide ions, which may improve the mobility of the conducting species. In the sulfide glasses, high conductivity values of 10^{-4}-10^{-3} Scm^{-1} at room temperature were obtained in the Li_2S-SiS_2-LiI [1-41, 77] and Li_2S-SiS_2-Li_3PO_4 [1-42]. Secondly, applying the ionic conductors as solid electrolytes in all solid-state batteries, the necessary characteristics for the use of practical batteries are as the follows:

- Wide potential window
- Chemical stability

Low reduction potential and high decomposition potential of the ionic conductors are important characters for the use of solid electrolytes. The oxidation-reduction reactions are normally caused by the *d*-electron in the transition elements. In order to achieve high electrochemical stability, it is preferable to use the materials which do not include the transition elements for solid electrolytes. Chemical stability is also important characteristics for the solid electrolytes. By considering these characteristics, sulfides with no transition elements might be the best candidate for the solid electrolytes of all solid-state cells. In the search for lithium ion conducting

solid electrolytes, Kanno and Irie *et al*. initiated the preliminary studies on the materials search based on the germanium sulfides systems,Li_2S-GeS_2, Li_2S-GeS_2-ZnS, and Li_2S-GeS_2-Ga_2S_3 [1-78], and in the ternary Li_2S-GeS_2-Ga_2S_3 system, a high ionic conductivity area was firstly found. The X-ray diffraction patterns of the solid solution system were found to be the similar patterns to the oxide LISICON ($Li_{14}Zn(GeO_4)_4$) found by Hong [1-58], which indicates that the materials with the same structure as the oxide LISICON exist in the sulfides. They were named the system "Thio-LISICON". With the discovery of thio-LISICON, many new materials were expected by aliovalent substitutions. $Li_{3.35}Ge_{0.35}P_{0.65}S_4$, thio-LISICON family, shows the highest conductivity of 1.2 x 10^{-2} Scm^{-1} at room temperature of any sintered ceramic materials [1-79]. In the present study, sulfide-based solid electrolyte with general formula $Li_{4-x}Ge_{1-x}P_xS_4$ included $Li_{3.35}Ge_{0.35}P_{0.65}S_4$ was examined to evaluate the germanium content in $Li_{4-x}Ge_{1-x}P_xS_4$.

1.10 Application to all solid-state lithium battery – thin film type and bulk type –

There are two types of all solid-state lithium batteries, solid state lithium batteries with thin film electrolyte and solid state batteries with bulk electrolyte [1-80]. Ionic conductivity of thin film electrolyte used thin film type batteries is 10^{-4} Scm^{-1} at room temperature. The thickness of the unit cell is about 1 mm. There are such as $Li_{3.4}Si_{0.6}P_{0.4}O_4$ (LISICON) [1-81] and $Li_{3-x}PO_{4-y}N_y$ (LiPON) [1-82] as the thin film electrolytes. The thin film type battery is generally synthesized by radio frequency (RF) magnetron sputtering and e-beam evaporation [1-83, 84], and the interface at the electrode/electrolyte is formed by the scale of atom scale [1-85]. The excellent cycle performances over a few million cycles and rate characteristics over 20 C (over 10 mA cm^{-2}) have been reported due to the contact of the atomic scale at the electrode/electrolyte interface [1-86, 87]. On the other hand, Ionic conductivity of bulk

electrolyte used bulk type batteries is over 10^{-4} Scm^{-1} at room temperature [1-42, 57]. There are such as $Li_{3x}La_{2/3-x}TiO_3$ [1-57] and Li_3PO_4-SiS_2-Li_2S [1-42] as the bulk electrolytes. The bulk is generally formed by scale of particle size [1-87, 88]. The bulk type solid-state battery shows the excellent cycle performance at low current density although the rate characteristics are not well [1-88]. All solid-state lithium batteries with solid ceramic electrolytes besides thio-LISICON have been reported at low current densities [1-78]. The thin film type solid-state lithium battery is superior to bulk type solid-state lithium battery in terms of the cycle performance and rate characteristics. However, the bulk type solid-state lithium battery has been expected to apply for larger scale lithium batteries, EV, HEV, etc. The thin film type solid-state batteries have small energy density for practical use.

The solid-state batteries are composed of three main components, electrolyte, anode, and cathode. Each component has the issue for practical use in the all solid-state lithium batteries.

1.11 Research trend for ceramic lithium solid electrolyte

The important issues of ceramic solid electrolyte are ionic conductivity, potential windows, transport number, chemical stability. The sulfide-based solid electrolytes have been reported in Japan. There are two types of the sulfide-based solid electrolyte; glass materials and crystalline materials. Both materials show the high ionic conductivities over 10^{-3} Scm^{-1} at 25˚C, and the high potential windows range. Li_3PO_4-Li_2S-SiS_2 glass is one of typical glass electrolytes [1-42]. The glass electrolyte of the Li_2S-P_2S_5 system also has ionic conductivity over 10^{-4}-10^{-5} Scm^{-1} at room temperature [1-89, 90]. The glass-ceramics has the high ionic conductivity of 3.2×10^{-3} Scm^{-1} at room temperature [1-91, 92]. The thio-LISICON family, with the general formula $Li_xM_{1-y}M'_yS_4$ (M=Si, Ge, and M'= P, Al, Zn, Ga, Sb), have the framework structure of the g-Li_3PO_4 type, and their ionic conductivities are in the order

of 10^{-7} – 10^{-3} S cm^{-1} at room temperature [1-78, 79, 93, 94]. Among the materials synthesized, the thio-LISICON based on the lithium germanium phosphorus sulfide ($Li_{3.35}Ge_{0.35}P_{0.65}S_4$) was found to show the highest conductivity of 1.2×10^{-2} Scm^{-1} at room temperature. This conductivity is comparable to the values obtained using organic electrolytes [1-95]. Thio-LISICON family also provide a wide potential window with a high decomposition potential of -5V (*vs*. Li/Li^+), which is suitable for practical use in all solid-state batteries [1-95, 96]. Similarly, Li_2S-P_2S_5 system has the high ion conductivity. Ionic conductivity of $Li_{3.325}P_{0.935}S_4$ has the highest value (1.5×10^{-4} Scm^{-1} at room temperature) in the $Li_{3+5x}P_{1-x}S_4$ solid solution [1-49, 97]. The issues for ceramic solid electrolyte are also chemical stability and electrochemical stability. The relationship of ionic conductivity, structure, and phase in lithium ionic conductors must be analyzed in order to realize solid-state lithium battery. There are few useful reports studied the relationship between ionic conductivity and phase in crystalline lithium-ion conductors [1-49, 51], conduction mechanism by first principles calculations [1-98], the relationship between ionic conduction, structure, and lithium concentration based on the structural an d electrochemical information [1-99].

1.12 Research trend for cathode materials

Lithium cobalt layer, $LiCoO_2$ has mainly been used as the cathode in all solid-state lithium batteries [1-100, 101]. $LiCoO_2$ is also used as cathode for bulk type batteries. The bulk type batteries have a good cycle performances over a few hundreds at a low current density of 64 μAcm^{-2} [1-89, 90]. To improve the rate characteristics in solid-state bulk batteries, mixing in cathode active materials and conductive materials is optimized; conductive materials of acetylene black, titanium, the ball-milling conditions, and the particle sizes of solid electrolyte and active material [1-103, 104, 105]. Solid electrolytes can effectively suppress the side reactions that deteriorate battery performances unlike liquid electrolyte because solid electrolytes have a wide electrochemical potential window. The suppression of reactions at the electrode/electrolyte interface is effective approach to improve cycle

performance. That modification of interface also improves rate characteristics and thermal stability. [1-106]. $LiCoO_2$ coated with some materials to modify at cathode/electrolyte interface were studied, coated with Al_2O_3, ZrO_2, SiO_2, $AlPO_4$, Li_2Si_3, $LiNbO_3$ [1-107, 108, 109, 110, 111, 112, 113, 114]. On the other hand, sulfur is one of the attractive materials as cathode in all solid-state batteries. Sulfur has larger theoretical capacity than conventional cathode materials, $LiCoO_2$. The loss of active material in liquid electrolytes caused low active material utilization and poor cycle performance for the Li/S cells. Therefore, sulfur cannot be applied for lithium batteries with liquid electrolyte. On the other hand, sulfur has possibility as cathode in solid-state battery. One of the issues using sulfur as cathode in solid-state batteries is the poor electric conductivities. Researchers were studied to improve the electric conductivities of sulfide, mechanically milled mixtures of sulfur and transition metal sulfides [1-115], the composite electrode of sulfur and AB mixed by ball milling [1-116], core shell structured Li_2S nanoparticles with Li_2S core and Li_3PS_4 as the shell [1-117]. All solid-state batteries using sulfur as cathode and ceramic solid electrolyte have been recently reported to have good cycle performance [1-118]. All solid-state lithium batteries with them are very attractive compared to lithium-ion batteries with liquid electrolyte using only limited cathode materials such as $LiCoO_2$, $LiMn_2O_4$, and $LiFePO_4$ [1-119, 120].

1.13 Research trend for anode materials

Among many anode materials in lithium batteries, lithium metal is one of the most attractive negative electrodes. Lithium metal has the lowest potential of 0 V (*vs* Li/Li^+) in the system and the largest capacity of 3,861 $mAhg^{-1}$. Lithium metal is utilized for the thin-film type lithium batteries with LIPON as solid electrolyte [1-82]. These thin-film type batteries showed the excellent cycle performance over a few million [1-103], which is shown that the interface at lithium metal and LIPON is electrochemically stable in the charge-discharge process without any side reactions. On the other hand, in the all solid-state bulk type lithium batteries with sulfides-based solid electrolyte, lithium-indium alloy and lithium-aluminum alloy have

been so far utilized as negative electrode [1-122, 123, 124, 125]. The all solid-state lithium batteries with lithium-indium alloy and lithium-aluminum alloy as negative electrode have ever reported with the good cycle performance [1-124, 125, 126]. The most widely negative electrode material in lithium batteries is now graphite. The graphite has good cycle performance with a theoretical capacity of 372 $mAhg^{-1}$. On the other hand, other group IV semiconductors, Sn and Si, are attractive materials as negative electrode. Sn and Si can offer significantly higher capacities: 990 $mAhg^{-1}$ for $Li_{4.4}Sn$ and 4200$mAhg^{-1}$ for $Li_{4.4}Si$ [1-127, 128]. In addition to the large increase in energy storage capacity, lithium-M alloys (Li_y-M, M= Sn, Si) also have a safe thermodynamic potential, making them attractive candidates for negative electrodes of lithium batteries [1-129]. Especially, there is great hope that interface of tin negative electrode/solid electrolyte is strongly contact because tin metal has high ductility. Negative electrode materials with higher potentials than Li metal is comfortable to high electrochemical stability at electrode/electrolyte interface because it has high possibility for solid electrolyte to be decomposed at the interface Li metal and solid electrolyte. However, the electrochemical behavior of all solid-state lithium batteries using Li_y-M (M=Sn, Si) alloy with wide redox potential range has not reported as ever. Li_y-Sn alloy and Li_y-Si alloy show redox potential, 0.4-0.8 V and 0.4-0.6 V (*vs* Li/Li^+), respectively. These alloys have possibility to work as negative electrode with suitable redox potential.

1.14 Research trend for solid electrode/solid electrolyte interface

The lithium ion migration was relatively slow at the electrode/electrolyte interface in solid-state batteries compared to the batteries with liquid electrolyte. This is because the liquid electrolyte can penetrate into solid electrolyte and have the electrochemical reaction area expanded due to fluidity of liquid. On the other hand, the

electrochemical reaction area in solid-state battery is extensively small because solid electrolyte is difficult to penetrate into the solid electrode [1-130]. The advantage of all solid-state lithium battery does not contain the electrochemical reaction such (de-)solvation of lithium ion at electrode/electrolyte interface using liquid electrolyte [1-131]. Therefore, the lithium ion is expected to be migrated through the electrode/electrolyte interface to construct tightly contact of solid/solid materials. The all solid-state batteries have the both cathode/electrolyte interface and anode/electrolyte interface as shown Figure 1-7. For the former interface, any researchers have recently reported the improvement to suppress the space charge layer at the interface [1-113, 132, 133, 134], the relationship between electrode structure and electrochemical properties based on the physical stress of the cathode/electrolyte interface [1-135]. Increase of electrochemical reaction area was carried out by the trial of micro-particle and conductive materials with larger surface area. For the latter interface, little effort has conducted to clarify the mechanism at the interface. As described in above section, lithium-indium alloy and lithium-aluminum alloy have been utilized for the negative electrode in all solid-state lithium batteries with sulfide-based solid electrolyte.

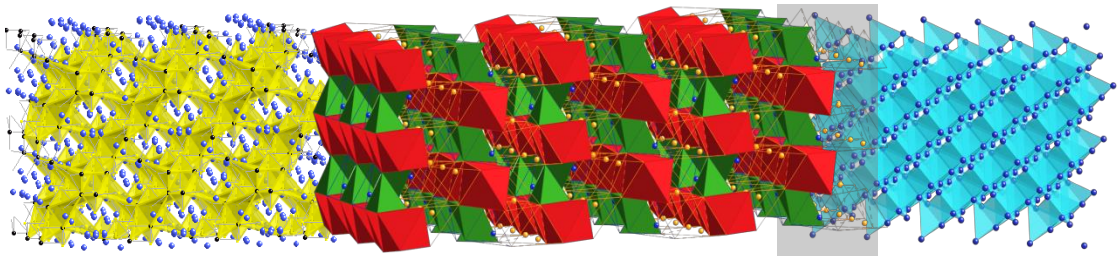

Figure 1-7 Schematic drawing of all solid-state battery with thio-LISICON electrolyte.

1.15 Research trend for development of industrialized solid-state battery

All solid-state batteries are an important technique for large scale device. With regard to both safety and reliability, all solid-state lithium batteries incorporating non-flammable solid electrolytes are one of the most promising candidates. Performance improvements, such as a higher energy density and sufficient power density, are important. Researchers also focus on improving cycle performance and storage life over today's lithium batteries with solid electrolyte. Though all solid-state batteries have many good points for enlargement of battery systems, there are still a lot of issues that should be solved to market it, volume change of electrodes, poor processing workability and formability. In addition to materials development of batteries, configuration of all solid-state battery and manufacturing technology such as thin film formation, particle dispersion and mixing is being developed recently. However, all solid-state battery with a volumetric energy density about twice that of conventional lithium-ion batteries is demonstrated in 2012 by the Toyota all solid-state battery [1-136].

1.16 Purpose of this study

In the present study, reaction at electrode/electrolyte interface (SEI) of all solid-state batteries were studied for combinations of sulfide-based solid electrolytes with various $Li_{4-x}Ge_{1-x}P_xS_4$, thio-LISICON, and Li_y-M (M=Sn, Si) alloy as negative electrode using AC impedance X-ray diffraction, and energy dispersive X-ray spectroscopy. The formation of the SEI layer at the electrode/electrolyte interface is an important factor in stabilizing the charge-discharge reactions in cells incorporating sulfide-based solid electrolytes. The optimization of the interface by the appropriate choice of electrode and electrolyte materials is important for the future development of all-solid-state batteries.

To achieve lower resistivity and higher stability of the SEI layer, novel

lithium ion conductive oxy-sulfides with the LGPS structure were searched in a ternary diagram of Li_2S-P_2S_5-P_2O_5 system and its structure and electrochemical properties were investigated. The SEI resistance of Li-P-S-O systems in symmetrical cell was also evaluated via charge-discharge and ac-impedance measurements.

References

[1-1] M. Wakihara, *Mater. Sci. Eng.*, **R33**, 109 (2001).

[1-2] Secondary battery sales statistics by volume and by value, The Battery Association of Japan.

[1-3] The actual situation and the future prospects of the battery industry (2013), Japan economic center.

[1-4] N. Terada, T. Yanagi, S. Arai, M. Yoshikawa, K. Ohta, N. Nakajima, A. Yanai, and N. Arai, *J. Power Sources,* **100**, 80 (2001).

[1-5] K. Zaghib, P. Charest, A. Guerfi, J. Shim, M. Perrier, and K. Striebel, *J. Power Sources,* **134**, 124 (2004).

[1-6] Catalogue Handbook of Fine chemicals, Aldrich Chemical Company, Inc., Wissconsin, USA (1988-1989).

[1-7] B. K. Mandal, A. K. Padhi, Z. Shi, S. Chakraborty, and R. Filler, *J. Power Sources,* **162**, 690 (2006).

[1-8] S.C. Levy, P. Bro, Battery Hazards and Accident Prevention, Plenum, New York, 1994.

[1-9] P.G. Balakrishnan, R. Ramesh, and T. Prem Kumar, *J. Power Sources,* **155**, 401 (2006).

[1-10] Macworld **36,** 12 (1995).

[1-11] Los Angeles Times, September 15, 1995, p. 1D.

[1-12] Dagens Industri, January 12, 1996, p. 10.

[1-13] www.bccresearch.com, September 2004.

[1-14] M. Kise, S. Yoshioka, and H. Kuriki, *J. Power Sources,* in press.

[1-15] M. Wu, P. J. Chiang, J. Lin, and Y. Jan, *Electrochimica Acta,* **49**, 1803 (2004).

[1-16] H. Kweon, J. Park, J. W. Seo, G. B. Kim, B. H. Jung, and H. S. Lim, *J. Power Sources,* **126**, 156 (2004).

[1-16] D.Y. Lee, H.S. Lee, H.S. Kim, H.Y. Sun, and D.Y. Seung, Korean, *J. Chem. Eng.*, **19**, 645 (2002).

[1-18] G. Oraädd, L. Edman, and A. Ferry, *Solid State Ionics*, **152-153**, 131 (2002).

[1-19] S. Lee, S. Kim, and S. Ahn, *J. Power Sources*, in press.

[1-20] T. Welton, Chem. Rev. (Washington, D.C.), **99**, 2071 (1999).

[1-21] M. Galinski, A. Lewandowski, and I. Stepniak, *Electrochimica Acta*, **51**, 5567 (2006).

[1-22] H. Tokuda, K. Hayamizu, K. Ishii, M. A. B. H. Susan, and M. Watanabe, *J. Phys. Chem. B*, **108**, 16593 (2004).

[1-23] H. Tokuda, K. Hayamizu, K. Ishii, M. A. B. H. Susan, and M. Watanabe, *J. Phys. Chem. B*, **109**, 6103 (2005).

[1-24] Y. Kato, K. Suwa, H. Ikuta, Y. Uchimoto, M. Wakihara, S. Yokoyama, T. Yabe and M. Yamamoto, *J. Mater. Chem.*, **13**, 280 (2003).

[1-25] S. Seki, Y. Ohno, Y. Kobayashi, H. Miyashiro, A. Usami, Y. Mita, H. Tokuda, M. Watanabe, K. Hayamizu, S. Tsuzuki, M. Hattori, and N. Terada, *J. Electrochem. Soc.*, **154 (3)**, A173 (2007).

[1-26] K. Takada, T. Inada, A. Kajiyama, H. Sasaki, S. Kondo, M. Watanabe, M. Murayama, and R. Kanno, *Solid State Ionics,* **158**, 269 (2003).

[1-27] H. Yamane, M. Shibata, Y. Shimane, T. Junke. Y. Seino, S. Adams, K. Minami, A. Hayashi, M. Tatsumisago, *Solid State Ionics*, **178**, 1163 (2007).

[1-28] R. Kanno, M. Murayama, *J. Electrochem. Soc.*, **148(7)**, A742 (2001).

[1-29] E. Z. Monikowska, Z. Florjañczyka, A. Tomaszewska, M. Pawlicka, N. Langwald, R. Kovarsky, H. Mazor, D. Golodnitsky, E. Peled, *Electrochimica Acta,* **53**, 1481 (2007).

[1-30] P. Mustarelli, E. Quartarone, C. Capiglia, C. Tomasi, P. Ferloni, and A. Magistris, *J. Chem. Phys.*, **111**, 3761 (1999).

[1-31] C. S. Kim, and S. M. Oh, *Electrochimica Acta*, **45**, 2101 (2000).

[1-32] M. Saito, H. Ikuta, Y. Uchimoto, M. Wakihara, S. Yokoyama, T. Yabe, and M. Yamamoto, *J. Electrochem. Soc.,* **150(6)**, A726 (2003).

[1-33] J. B. Kerr, Y. B. Han, G. Liu, C. Reeder, J. Xie, and X. Sun, *Electrochemica*

Acta, **50**, 235 (2004).

[1-34] B. Scrosati, F. Croce, and S. Panero, *J. Power Sources*, **100**, 93 (2001).

[1-35] J. M. Tarascon and M. Armand, *Nature* (London), **414**, 359 (2001).

[1-36] C. Julien and M. Balkanski, in Thin Film Microbatteries, M. Balkanski, Editor, p. 3, North Holland, Amsterdam, (1991).

[1-37] K. Iwamoto , N. Aotani, K. Takada, and S. Kondo, *Solid State Ionics*, **79**, 288 (1995).

[1-38] T. Kudo, "*Solid State Ionics"* (eds. T. Kudo, and K. Fueki), Chap. 1, Kodansha, Tokyo (1990).

[1-39] J. Kuwano, and M. Kato, *Denki Kagaku*, **46**, 353 (1978).

[1-40] D. O. Raleigh, *J. Appl. Phys.*, **41**, 1876 (1970).

[1-41] J. H. Kennedy, and Y. Yang, *J. Solid State Chem.*, **69**, 252 (1987).

[1-42] S. Kondo, K. Takada, and Y. Yamamura, *Solid State Ionics*, **53-56**, 1183 (1992).

[1-43] K. Hirai, M. Tatsumisago, and T. Minami, *Solid State Ionics*, **78**, 269 (1995).

[1-44] K. Miyauchi *et al*., Extended Abs. 161st Electrochem. Soc. Meet. (Montreal), p. 1138 (1982).

[1-45] M. Tatsumisago, N. Machida, and T. Minami, *J. Ceran. Soc. Jpn.*, **95**, 197 (1987).

[1-46] K. Iwamoto, N. Aotani, K. Takada, and S. Kondo, *Solid State Ionics*, **70-71**, 658 (1994).

[1-47] K. Iwamoto, N. Aotani, K. Takada, and S. Kondo, *Solid State Ionics*, **79**, 288 (1995).

[1-48] K. Takada, K. Iwamoto, and S. Kondo, *Solid State Ionics*, **117**, 273 (1999).

[1-49] M. Tachez, J-P. Malugani, R. Mercier, and G. Robert, *Solid State Ionics*, **14**, 181 (1984).

[1-50] B. T. Ahn, and R. A. Huggins, *Mater. Res. Bull.*, **24**, 889 (1989).

[1-51] B. Wang, B. C. Chakoumakos, B. C. Sales, B. S. Kwak, and J. B. Bates, *J.*

Solid State Chem., **115**, 313 (1995).

[1-52] W. Gratzer, H. Bittner, H. Nowotny, and K. Seifert, *Z. Kristallgr.*, **133**, 260 (1971).

[1-53] C. R. Schlaikjer, and C. C. Liang, "*Fast Ion Transport in Solids"* (ed. W. van Gool), p. 685, North-Holland, Amsterdam (1973).

[1-54] T. Lapp, S. Skaarup, and A. Hooper, *Solid State Ionics*, **11**, 97 (1983).

[1-55] M. S. Whittingham, and R. A. Huggins, *National Burean of Standard* (*NBS*) *Spec. Publ.*, **364** (Solid State Chem.), 139, (1972).

[1-56] R. Kanno, Y. Takeda, A. Matsumoto, and O. Yamamoto, *J. Solid State Chem.*, **75**, 41 (1988).

[1-57] Y. Inaguma, L. Chen, M. Itou, and T. Nakamura, *Solid State Ionics*, **70-71**, 203 (1994).

[1-58] H. Y-P. Hong, *Mater. Res. Bull.*, **13**, 117 (1978).

[1-59] J. Kuwano, and A. R. West, *Mater. Res. Bull.*, **15**, 1661 (1980).

[1-60] Y-W. Hu, I. D. Raistrick, and R. A. Huggins, *J. Electrochem. Soc.*, **124**, 1240 (1977).

[1-61] J. Kuwano, M. Nagamine, M. Higuchi, and M. Kato, *Denki Kagaku*, **49**, 667 (1981).

[1-62] R. A. Huggins, *Electrochimica Acta*, **22**, 773 (1977).

[1-63] A. Rabenau, *Solid State Ionics*, **6**, 277 (1982).

[1-64] J. M. Newsam, and A. K. Cheetham, *J. Solid State Chem.*, **60**, 214 (1985).

[1-65] A. R. West, *Z. Kristallgr.*, **141**, 422 (1975).

[1-66] R. I. Smith, and A. R. West, *J. Solid State Chem.*, **93**, 436 (1991).

[1-67] A. Joffé, *Ann. Phys.* (*Leibzig*), **72**, 461 (1923).

[1-68] J. Frenkel, *Z. Phys*., **35**, 652 (1926).

[1-69] C. Wagner, and W. Schotthy, *Z. Phys. Chem*., **B11**, 163 (1930).

[1-70] C. Wagner, *Naturwissenschaften*, **31**, 265 (1943).

[1-71] T. Takahashi, O. Yamamoto, S. Yamada, and S. Hayashi, *J. Electrochem.*

Soc., **126**, 1654 (1979).

[1-72] R. Kanno, K. Ohno, Y. Kawamoto, Y. Takeda, O. Yamamoto, T. Kamiyama, H. Asano, F. Izumi, and S. Kondo, *J. Solid State Chem.*, **102**, 79 (1993).

[1-73] A. R. West, "*Solid State Electrochemistry"* (ed. P. G. Bruce), Chap. 2, Cambridge University Press, Cambridge, UK (1995).

[1-74] S. Kondo, "*Lithium Ion Batteries"* (eds. M. Wakihara, and O. Yamamoto), Chap. 9, Kodansha, Tokyo (1998).

[1-75] J. N. Bradly, and P. D. Green, *Trans. Faraday*, **62**, 2069 (1965).

[1-76] B. B. Owens, and G. R. Argue, *Science*, **157**, 308 (1967).

[1-77] R. Kanno, Y. Takeda, K. Takada, and O. Yamamoto, *J. Electrochem. Soc.*, **131**, 469 (1984).

[1-78] R. Kanno, T. Hata, Y. Kawamoto, and M. Irie, *Solid State Ionics*, **130**, 97 (2000).

[1-79] R. Kanno, and M. Murayama, *J. Electrochem. Soc.*, **148**, A742 (2001).

[1-80] R. Kanno, *Electrochemistry*, **71(8)**, 710 (2003).

[1-81] J. F. Whitacre, and W. C. West, *Solid State Ionics*, **175**, 251 (2004).

[1-82] J. Schwenzel, V. Thangadurai, and W. Weppner, *J. Power Sources*, **154**, 232 (2006).

[1-83] W. Liu, Z. Fu, and Q. Qin, *Thin Solid Films*, **515**, 4045 (2007).

[1-84] C. Li, B. Zhang, and Z. Fu, *Thin Solid Films*, **515**, 1886 (2006).

[1-85] J. M. Lee, S. H. Kim, Y. Tak, and Y. S. Yoon, *J. Power Sources*, **163**, 173 (2006).

[1-86] H. Y. Park, S. C. Nam, Y. C. Lim, K. G. Choi , K. C. Lee , G. B. Park, J. B. Kim , H. P. Kim, and S. B. Cho, *Electrochimica Acta,* **52**, 2062 (2007).

[1-87] N. Machida, *J. Jpn. Soc. Powder Powder Metallurgy,* **52 (8)**, 589 (2003).

[1-88] F. Mizuno, A. Hayashi, K. Tadanaga, and M. Tatsumisago, *Solid State Ionics*, **177**, 2731 (2006).

[1-89] A. Hayashi, K. Iio, H. Morimoto, T. Minami, and M. Tatsumisago, *Solid State*

Ionics, **175**, 637 (2004).

[1-90] T. Ohtomo, F. Mizuno, A. Hayashi, K. Tadanaga, and M. Tatsumisago, *Solid State Ionics*, **176**, 2349 (2005).

[1-91] F. Mizuno, A. Hayashi, K. Tadanaga, and M. Tatsumisago, *Adv. Mater.* **17**, 918 (2005).

[1-92] K. Minami, F. Mizuno, A. Hayashi, and M. Tatsumisago, *Solid State Ionics*, **178**, 837 (2007).

[1-93] M. Murayama, R. Kanno, M. Irie, S. Ito, T. Hata, N. Sonoyama, and Y. Kawamoto, *J. Solid State Chem.*, **168**, 140 (2002).

[1-94] M. Murayama, R. Kanno, Y. Kawamoto, and T. Kamiyama, *Solid State Ionics*,**154-155**, 789 (2002).

[1-95] N. Kamaya, K. Homma, Y. Yamakawa, M. Hirayama, R. Kanno, M. Yonemura, T. Kamiyama, Y. Kato, S. Hama, K. Kawamoto and A. Mitsui, *Nat. Mater* 10(2011) (9), p.682.

[1-96] T. Inada, T. Kobayashi, N. Sonoyama, A. Yamada, S. Kondo, M. Nagao and R. Kanno, *J. Power Sources* 194 (2009) (2), p. 1085

[1-97] M. Murayama, N. Sonoyama, A. Yamada, and R. Kanno, *Solid State Ionics*, **170**, 173 (2004).

[1-98] Y..Mo, S. P. Ong, G. Ceder, *Chem. Mater*. 24(2012)15-17

[1-99] S. Hori, K. Suzuki, M. Hirayama, Y. Kato, T. Saito, M. Yonemura, R. Kanno, *Faraday Discussions*, 2014, 176, 83-94

[1-100] N. Ohta, K. Takada, L. Zhang, R. Ma, M. Osada, and T. Sasaki, *Adv. Mater.* **18**, 2226 (2006).

[1-101] T. Minami, A. Hayashi, and M. Tatsumisago, *Solid State Ionics*, **177**, 2715 (2006).

[1-102] N. Terada, T. Yanagi, S. Arai, M. Yoshikawa, K. Ohta, N. Nakajima, A. Yanai, and N. Arai, *J. Power Sources,* **100**, 80 (2001).

[1-103] F. Mizuno, A. Hayashi, K. Tadanaga, and M. Tatsumisago, *J. Electrochem. Soc.*

152(8), A1499 (2005).

[1-104] Y. Inda T. Katoh, and M. Baba, *J. Power Sources*, **174**, 741 (2007).

[1-105] H. Sasaki, K. Takada, T. Inada, A. Kajiyama, S. Kondo, and M. Watanabe, *J.Power Sources*, **119-121**, 774 (2003).

[1-106] A. Sakuda, A.Hayashi, and M.Tatsumisago, Chem. Mater., 2010, 22, 949-956

[1-107] J. Cho, Y.-J. Kim, B. Park, *Chem. Mater.* 2000, 12, 3788–3791

[1-108] J. Cho, Y.-J. Kim, J.-T. Kim, B. Park, *Angew. Chem., Int. Ed.*2001, 40, 3367–3369

[1-109] J. Cho, B. Kim, J.-G. Lee, Y.-W. Kim, B. J. Park, *Electrochem.Soc*. 2005, 152, A32–A36

[1-110] Z. Chen, J. R. Dahn, *Electrochem. Solid-State Lett*. 2003, 6, A221–A224

[1-111] Z. Chen, J. R. Dahn, *Electrochim. Acta* 2004, 49, 1079–1090.

[1-112] Sun, Y.K. Cho, S.W. Myung, S.T. Amine, K. Prakash, J.Electrochim. Acta. 2007, 53, 1013–1019.

[1-113] A. Sakuda, H. Kitaura, A. Hayashi, K. Tadanaga and M. Tatsumisago, *Chemical Materials article* 2010, 22, 949–956

[1-114] N. Ohta, K. Takada, I. Sakaguchi, L. Zhang, R. Ma, K. Fukuda, M. Osada, T. Sasaki, *Electrochemistry Communications* 9 (2007) 1486–1490

[1-115] A. Hayashi, T. Ohtomo, F. Mizuno, K. Tadanaga, M. Tatsumisago,*Electroshim. Acta*., 50 (2004) 893

[1-116] T. Kobayashi, Y. Imade, D. Shishihara, K. Homma, M. Nagao, R. Watanabe, T. Yokoi, A. Yamada, R. Kanno, T. Tatsumi, *Journal of Power Sources,* 182 (2008) 621–625

[1-117] Z. Lin, Z. Liu, N. J. Dudney, C. Liang, *ACS. Nano* 2013, 7, 2829 – 2833.

[1-118] N. Machida, K. Kobayashi, Y. Nishikawa, T. Shigematsu, *Solid State Ionics* 175 (2004) 247

[1-119] J. B. Goodenough, *J. Power Sources*, in press.

[1-120] S. Y. Chung, J. T. Bloking and Y. M. Chiang, *Nat. Mater.*, **1**, 123 (2002).

[1-121] B. J. Neudecker, R. A. Zuhr, and J. B. Bates, *J. Power Sources*, **81-82**, 27 (1999).

[1-122] K. Takada, N. Aotani, K. Iwamoto, and S. Kondo, *Solid State Ionics*, **86-88**, 877 (1996).

[1-123] F. Mizuno, A. Hayashi, K. Tadanaga, T. Minami, and M. Tatasumisago, *Solid State Ionics*, **175**, 699 (2004).

[1-124] R. Kanno, M. Murayama, T. Inada, T. Kobayashi, K. Sakamoto, N. Sonoyama, A. Yamada, S. Kondo, *Electrochemical and solid state letters, 7(12)* A455-A458(2004)

[1-125] T. Kobayashi, A. Yamada, R. Kanno, *Electrochimica Acta* 53(2008)5045-5050

[1-126] M. Nagao, H. Kitaura, A. Hayashi, M. Tatasumisago, *Journal of Power Sources* 189 (2009) 672–675

[1-127] C. M. Park, J.H. Kim, H.J. Sohn, *Chem. Soc. Rev.*, 2010, 39, 3115

[1-128] W.J. Zhang, *J. Power Sources*, 2011, 196, 13.

[1-129] C.-Y. Chou, H. Kim, and G.S. Hwang, *The Journal of Physical Chemistry* 2011, 115, 20018-20026

[1-130] F. Sagane, T. Abe, Y. Iriyama, and Z. Ogumi, *J. Power Sources,* **146**, 749 (2005).

[1-131] T. Abe, H. Fukunaga, Y. Iriyama, and Z. Ogumi, *J. Electrochem. Soc.*, **151 (8)**, A1120 (2004).

[1-132] N. Ohta, K. Takada, L. Zhang, R. Ma, M. Osada, and T. Sasaki, *Adv. Mater.* **18**, 2226 (2006).

[1-133] H. Kitaura, A. Hayashi, K. Tadanaga and M. Tatsumisago, *J. Electrochem. Soc.*, 2009, 156, A27. 9

[1-134] P. Verma, P. Maire, P. Novak, *Electrochimica. Acta.*, 55 (2010) 6332-6341

[1-135] K. Kishida, N. Wada, H. Adachi, K. Tanaka, H. Inui, C. Yada, Y. Iriyama, and Z. Ogumi, *Acta Materialia*, **55**, 4713 (2007).

[1-136] M. Chen, Y. Yan, W.-M. Liu, C. Zhou, Z.-Q. Guo, X.-F. Zhang, Y.-L. Wang, L.

Li, G.-L. Zhang, *Journal of Aeronautical Materials*, Volume 34, Number 6, 15 December 2014, pp. 1-20(20)

CHAPTER 2

Experimental

2.1 Sample preparation

Three sulfide-based solid electrolytes were used: $Li_{3.25}Ge_{0.25}P_{0.75}S_4$, $Li_{3.35}Ge_{0.35}P_{0.65}S_4$, and $Li_{3.5}Ge_{0.5}P_{0.5}S_4$, where the $Li_{4-x}Ge_{1-x}P_xS_4$ compositions in the ternary Li_2S-GeS_2-P_2S_5 system are represented by the formula LGPSx. The starting materials were Li_2S (Nihon Kagaku Kogyo), GeS_2 (Kojundo Chemical Laboratory, > 99.9% purity), and P_2S_5 (Aldrich, > 99% purity). These were weighed and mixed in appropriate molar ratios in an argon-filled glove box, and then they were enclosed in a vacuum using a carbon-coated quartz tube and heated at a fixed reaction temperature. After the reaction at a fixed temperature, the quartz tube was slowly cooled to room temperature. Each of these sulfide-based solid electrolytes was ground using a vibrating mill prior to the cell experiments. The synthetic processes by which these solid electrolytes were obtained have been described elsewhere [2-1, 2, 3].

2.2 Characterization by X-ray diffraction technique

The reaction products were characterized by X-ray diffraction technique. X-ray diffraction patterns of the samples were obtained with an X-ray diffractometer (Rigaku Smartlab) with CuKα radiation. The diffraction data were collected at each 0.03˚ step width over a 2θ range from 10 to 70˚. Figure 2-1 shows the constitution of the sample holder. The sample was mounted on a specially designed

X-ray holder in an argon atmosphere. The sample holder was covered by a polyimide film (Kapton) to prevent air and moisture contact during the measurement.

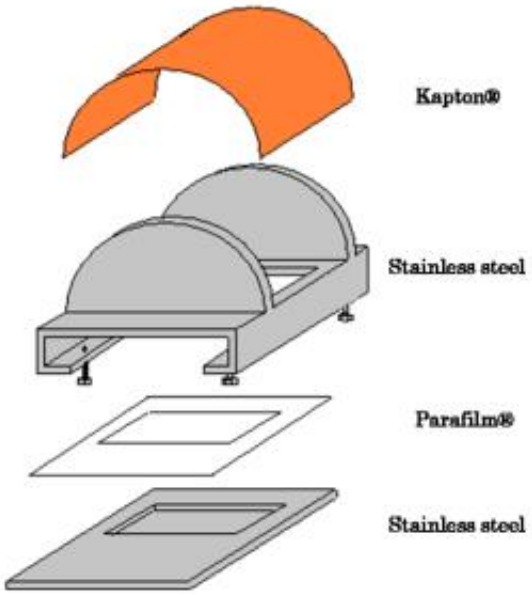

Figure 2-1 Sample folder for X-ray diffraction measurement

2.3 Physical property measurements

2.3.1 Charge-discharge measurement

For the charge-discharge test of all solid-state cells, the cathode was a mixture of $LiNbO_3$ -coated $LiCoO_2$ and thio-LISICON. The materials were weighted in the ratio of 60:40 (weight %), and mixed with a mortar for ten minutes. The test cell was composed of polyethylene terephthalate (PET) cylinder with an inner diameter of 10 mm. The solid electrolyte of about 70 mg was pressed into a pellet at 147 MPa. The cathode mixture of 10 mg was subsequently pressed onto one side of the electrolyte-pellet at 184 MPa in a dry argon-filled glove box ([H_2O] < 0.1ppm, Miwa MFG Co., Ltd.). The anode was applied with Li_y-M (M= Sn, Si) alloy. Sn powder

(99.8%, 325 mesh, Alfa Aesar) was pressed at 184 MPa and Li foil (0.6 mm thick, 6 mm diameter) was subsequently pressed onto the Sn layer at 9.2 MPa. Cells using a Li-Si alloy were also constructed via the same procedure but using Si powder (99.9%, 350 mesh, Nilaco) as the negative electrode material. The alloy compositions were varied by changing the ratios of Sn or Si to lithium metal in the electrodes. Figure 2-2 shows the layout of the measurement cell. The electrochemical properties of the cells were determined using a multi-galvanostat (TOSCAT-3100). A cycling test was performed between 0.5 and 4.2 V at an applied current of 64 μAcm^{-2} (0.05 C rate) at 25˚C.

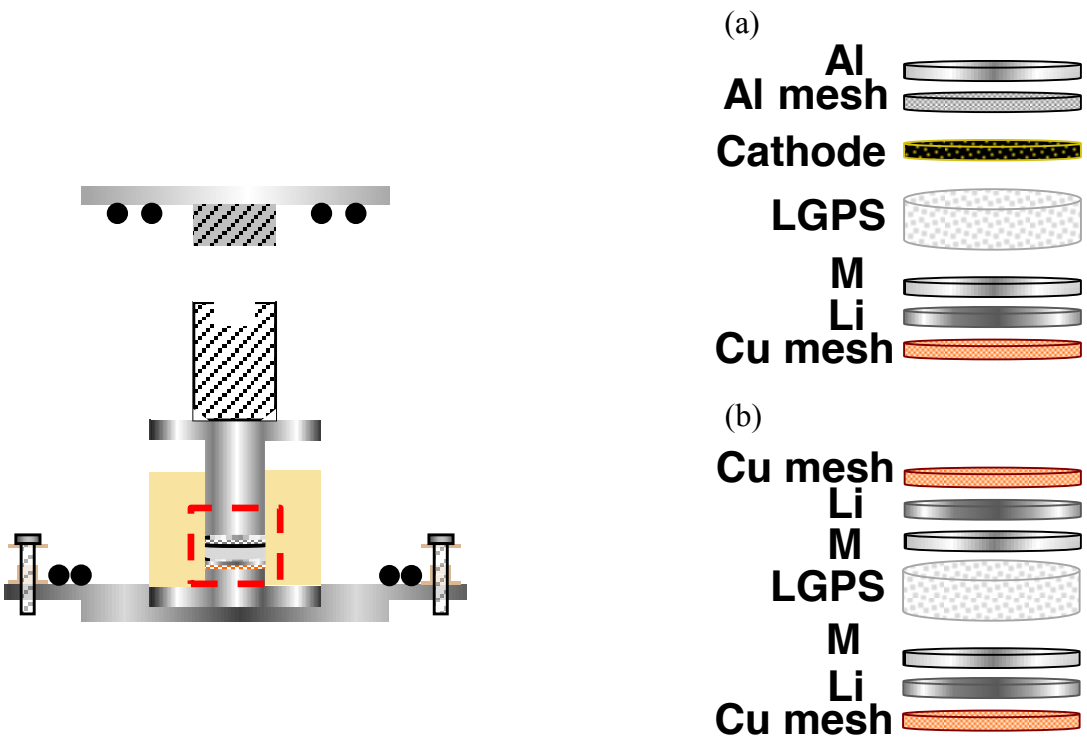

Figure 2-2 Physical property measurement cell (a)for charge-discharge, (b)for electrochemical measurement

2.3.2 Electrochemical measurement for model system

Symmetric cells with the configuration Li_y-M/solid electrolyte/M-Li_y (M=Sn, Si) were used for the resistance measurement. Each cell consisted of a polyethylene terephthalate (PET) cylinder with an inner diameter of 10 mm. A solid electrolyte sample of approximately 100 mg was pressed into a pellet at 147 MPa, following which Sn powder (99.8%, 325 mesh, Alfa Aesar) was pressed onto one side of the electrolyte pellet at 184 MPa and Li foil (0.6 mm thick, 6 mm diameter) was subsequently pressed onto the Sn layer at 9.2 MPa. Both electrodes had the same configuration, thus forming a symmetrical cell. Cells using a Li-Si alloy were also constructed via the same procedure but using Si powder (99.9%, 350 mesh, Nilaco) as the negative electrode material. Several alloy compositions with different Li/M (M=Sn, Si) ratios were examined to determine the relationship between the electrode redox potentials (*vs.* Li/Li^+) and the decomposition reactions. In these trials, the alloy compositions were varied by changing the ratios of Sn or Si to lithium metal in the electrodes. The test cell was similar configuration described above 2.3.1. Charge-discharge data were obtained with the symmetric cells by applying a constant current of 1.38 $mAcm^{-2}$ for 20 min, following which the same amount of current was applied after switching the current direction. After each cycle of the charge-discharge process, the AC impedance of the cell was measured. All the electrochemical experiments were carried out at room temperature (25 ºC). The resistances of the symmetrical cells were measured by the AC impedance measurements over an applied frequency range of 1 Hz to 1 MHz, using a frequency response analyzer (Solartron 1260) connected to an electrochemical interface (Solartron 1287). The software packages ZPLOT and ZVIEW were used for the measurements and the analyses, respectively [2-1].

Cell resistance was examined by AC impedance measurements. In solid electrolyte, symmetric cell is used without reference electrode. The AC impedance measurements is a method consisting in separating the bulk, grain boundary, and

electrode components of the measured sample, and then calculating the resistance-value by applying an AC voltage with the frequency change during the measurements. Also, the AC impedance measurements are hardly affected by the polarization and the interfacial reaction between the electrolyte and the electrode, this method is capable of measuring with high accuracy. When combining the equivalent circuits, there are three typical circuit elements which show different response to an AC signal. Table 2-1 shows three circuit elements; resistance, capacitor, and inductor. Their electrical properties are called resistance (R), capacitance (C), and inductance (L), respectively.

Table 2-1 Electrical properties of typical circuit elements.

Circuit element	Resistance	Capacitor	Inductor
Symbol, Unit	R, Ω	C, F	L, H
Phase shift	0˚	–90˚	90˚
Impedance	$Z_R = R$	$Z_C = (j\omega C)^{-1}$	$Z_L = j\omega L$

Furthermore, there exists a circuit element called Warburg impedance, represented by Z_w.

$$Z_w = A_w \omega^{-1/2}(1 - j) \qquad [A_w : \text{Warburg coefficient}]$$

Warburg impedance indicates the response characteristic which is caused by the diffusion process of the substance accompanying the electrode contribution, and the property in which the current is phase shifted –45˚ to the voltage with the magnitude proportional to $w^{-1/2}$.

Figure 2-3 shows an equivalent circuit, which is used in many cases, consisting of a simple *RC* element connected in parallel. The complex impedance, *Z** in Figure 2.3, is described by the following equation 2-1:

$$Z^* = \frac{R}{1+(\omega RC)^2} - jR\frac{\omega RC}{1+(\omega RC)^2} \qquad (2\text{-}1)$$

where

R : resistance,

C : capacitance,

ω : angular frequency,

j : imaginary number $(j = \sqrt{-1})$.

Above Equation 2-1 consists of the real and imaginary components, for example, $Z^* = Z' - jZ''$, where Z' and Z'' are the real and imaginary impedance components, respectively. Equation 2-1 may be transformed into Equation 2-2:

$$\left(Z' - \frac{1}{2}R\right)^2 + Z''^2 = \frac{1}{4}R^2 \qquad (2\text{-}2)$$

In Equation 2-2, if the imaginary part, Z'' are plotted as function of the real part, Z', a graph called "Nyquist plot" or "Cole-Cole plot", can be obtained. Figure 2-4 shows the Nyquist plot for the circuit in Figure 2-3. A semicircle is observed centered at (R/2, 0), the resistance-value is calculated from the diameter of the semicircle.

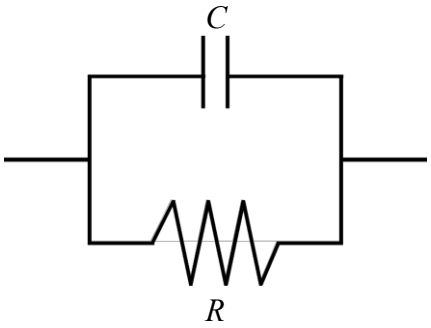

Figure 2-3 Simple circuit.

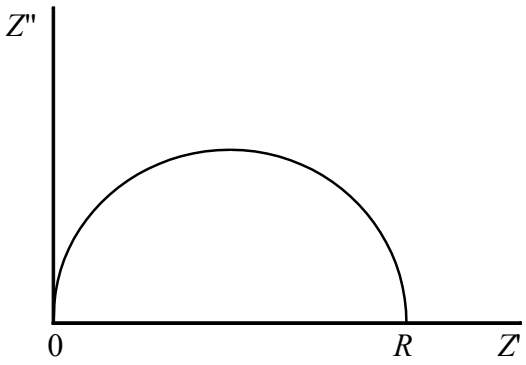

Figure 2-4 Nyquist plot for simple circuit.

2.3.3 X-ray diffraction measurement and Energy-dispersive X-ray spectroscopy

The electrolyte layers were removed from the cells following the resistance measurements, it is easy to separate the anode composite at the solid electrolyte/anode interface. The electrolyte surfaces were examined by XRD (Rigaku Smartlab) with CuKa radiation. The cross-sections of electrolyte samples were cut by ion-milling, and the surface regions of them were also analyzed using EDX (EDX, Genesis 4000).

References

[2-1] N. Kamaya, K. Homma, Y. Yamakawa, M. Hirayama, R. Kanno, M. Yonemura, T. Kamiyama, Y. Kato, S. Hama, K. Kawamoto and A. Mitsui, *Nat. Mater.*10 (2011) (9), p.682

[2-2] O. Kwon, M. Hirayama, K. Suzuki, Y. Kato, T. Saito, M. Yonemura, T. Kamiyama and R. Kanno, *Journal of Materials Chemistry,* A3 (2015) (1), p. 438

[2-3] R. Kanno, M. Murayama, *J. Electrochem. Soc.* 148 (2001) (7), p. A742

[2-4] *ZPLOT and ZVIEW for Windows, Scriner Associates Inc., North Carolina, USA* (1998).

CHAPTER 3

Reaction at the electrode/electrolyte interface with $Li_{4-x}Ge_{1-x}P_xS_4$

3.1 Introduction

With regard to both safety and reliability, all-solid-state lithium batteries incorporating non-flammable inorganic solid electrolytes are one of the most promising candidates. The most important component of such batteries is the electrolyte and one class of potential inorganic solid electrolytes exhibiting high ionic conductivities are the sulfide-based materials. All-solid-state lithium batteries incorporating solid electrolytes may provide a high energy and power density with suitable margins of safety. However, challenges related to fabricating electrochemical interfaces with a suitable degree of contact between the electrode and the electrolyte prevent the practical application of these materials in batteries. In the case of conventional liquid electrolyte-based batteries, the entire surface of the electrode is covered with the liquid electrolyte, which enables the electrochemical lithium (de)intercalation reaction to proceed readily over the whole interfacial region. In contrast, it is difficult to achieve close contact at the solid/solid interface in all-solid-state batteries because of the hard, brittle characteristics of inorganic solids [3-1]. Consequently, the resulting smaller electrode reaction area increases the interface resistance. It is therefore important to control the resistance of the electrode/solid electrolyte interface in all-solid-state batteries. Previous studies have examined the interfacial reactions of all-solid-state batteries using sulfide-based solid electrolytes belonging to the thio-LISICON family.

These studies found good cycle performance due to the formation of an interfacial phase at the electrode/electrolyte boundary during charge-discharge trials [3-1, 2]. When a current is applied to an all-solid-state battery, a solid electrolyte interphase (SEI) layer is formed at the interface between the thio-LISICON solid electrolyte and the electrode. In this chapter, reactions at the electrode/electrolyte interface of all solid lithium batteries were studied when using sulfide-based solid electrolytes, including the new electrolytes, $Li_{4-x}Ge_{1-x}P_xS_4$ (LGPSx) and Liy-M alloy as negative electrode.

3.2 Solid state configuration

$Li_{4-x}Ge_{1-x}P_xS_4$ of the thio-LISICON family was used as a solid electrolyte. The thio-LISICON has a structure similar to the γ-Li_3PO_4 type and a general composition of $Li_{4-x}M_{1-y}M'_yS_4$, where the M and M' are Ge, Si or P, Al, Ga, respectively [3-3, 4, 5]. Among these materials, $Li_{3.35}Ge_{0.35}P_{0.65}S_4$ has the highest conductivity of 1.2 x 10^{-2} Scm^{-1} at room temperature with the decomposition potential of above 5 V[3-6]. $LiNbO_3$-coated $LiCoO_2$ was used as a cathode. It has been reported that excellent cycle performance for cathode of lithium secondary battery [3-7]. The cathode was a mixture of $LiNbO_3$-coated $LiCoO_2$ and thio-LISICON with a mortar for ten minutes. Li_y-Sn alloys were used as an anode. Sn is useful since tin has a theoretical capacity of 990 mAh g^{-1}, which is approximately 2.7 times that of a carbon negative electrode (372 mAh g^{-1}) [3-8], while the high ductility of Sn might allow more intimate contact at the solid/solid interface. In addition, the higher lithium diffusion rate in Sn might improve the discharge rate characteristics of the system [3-9].

3.3 Charge-Discharge characteristics using $Li_{4-x}Ge_{1-x}P_xS_4$ and Liy-M (M=Sn, Si) negative alloys

Figure 3-1 shows the schematic drawing of the cell-design. The cell is composed of the electrolyte, multiple-layer anode, and the composite cathode. Copper mesh is applied as the electric collector for anode, and aluminum mesh and foil are applied as the electric collector for cathode. Figure 3-2(a) and (b) show the charge-and- discharge characteristics at a current density of 64μAcm^{-2} (0.05 C rate) in the potential range of 2.0 – 4.2 V at 25°C. In order to confirm the effect of the solid electrolyte composition, the cells with $Li_{3.25}Ge_{0.25}P_{0.75}S_4$ and $Li_{3.5}Ge_{0.5}P_{0.5}S_4$ were examined; the results are indicated in the same figure. Although capacity-fade was observed for two cells, low capacity and degradation with cycling was found for the cell with $Li_{3.5}Ge_{0.5}P_{0.5}S_4$. The causes of capacity-fade are considered the effect of the electrolyte composition and the effect of anode. Although Sn is known high capacity material, it suffers from poor cycleability during lithium insertion and extraction processes. In this study, the difference of low capacity and capacity-fade between Figure 3-2 (a) and Figure 3-2 (b) is caused by electrolyte composition, because the cells were applied with the same anode material: $Li_{0.4}Sn$ alloy. The capacity loss of the first discharge-and-charge cycle might be attributed to the current consumption by a phase change from the Sn to $Li_{0.4}Sn$ alloy. On the other hand, in evaluation of the effect of the electrode, Li_y-M (M=Sn, Si) alloy were used as an anode in this study. The effects of electrode composition were examined by varying the Li/M (M = Sn, Si) ratios in the electrodes. Figure 3-2 (a) and (c) show the charge-and-discharge characteristics at a current density of 64μAcm^{-2} (0.05 C rate) in the potential range of 2.0 – 4.2 V at 25°C. In order to confirm the effect of the electrode composition, the cells with $Li_{0.4}Sn$ and $Li_{3.5}Sn$ were examined. Although capacity-fade was observed for two cells, low capacity and degradation with cycling was found for the cell with $Li_{3.5}Sn$. In this study, the difference of low capacity and capacity-fade between Figure 3-2 (a) and Figure 3-2 (c) is caused by electrode composition, because the cells were applied with the same electrolyte material: $Li_{3.25}Ge_{0.25}P_{0.75}S_4$ electrolyte.

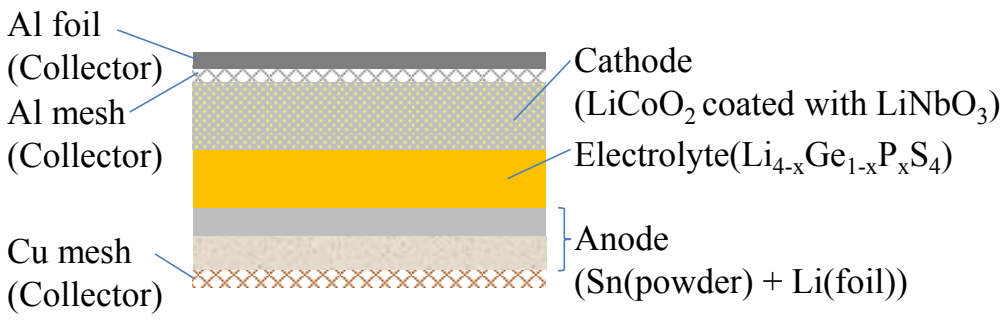

Fig.3-1 Schematic drawing of the cell configuration of all solid-state battery.

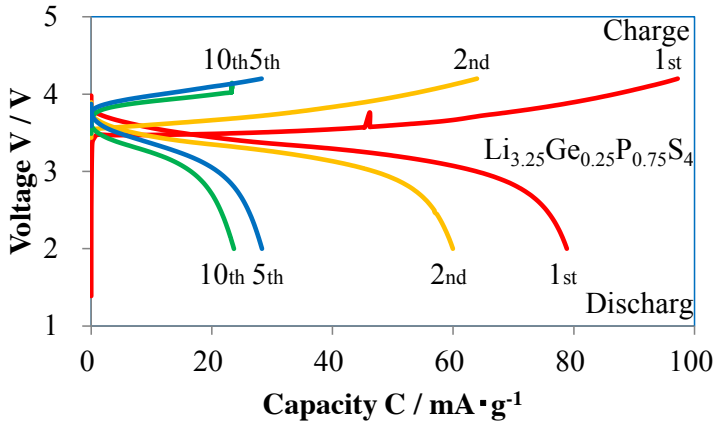

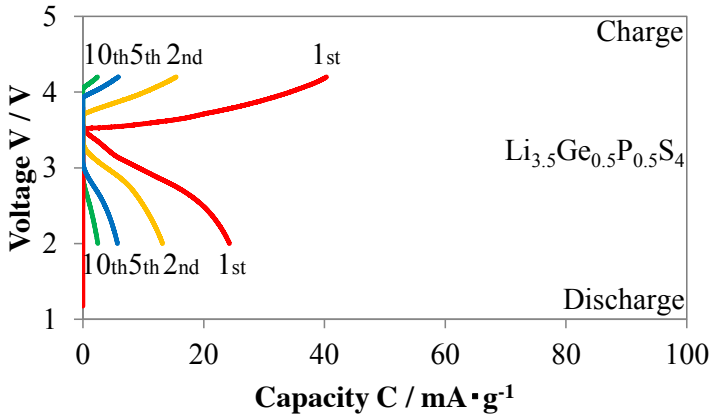

Fig.3-2 The $Li_{0.4}Sn/Li_{3.25}Ge_{0.25}P_{0.75}S_4$/Cathode cell showed cycling characteristic (a). The $Li_{0.4}Sn/Li_{3.5}Ge_{0.5}P_{0.5}S_4$/Cathode cell showed cycling characteristic (b).

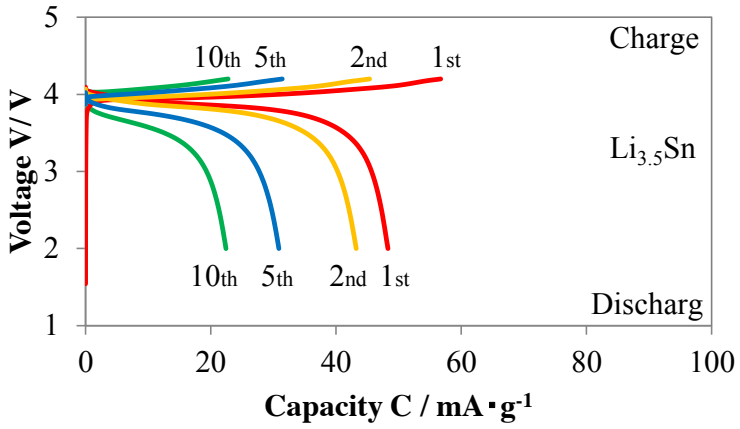

Fig.3-2 The $Li_{3.5}Sn$/ $Li_{3.25}Ge_{0.25}P_{0.75}S_4$ /Cathode cell showed cycling characteristic (c).

3.4 Relationship between SEI resistance and electrolyte composition

In order to clarify the effect of electrolyte composition for cycling, the anode/electrolyte interface has been measured by AC impedance measurement. Figure 3-4 presents a typical example of the plots obtained from AC impedance measurements during charge-discharge cycling. The impedance of symmetrical cells has previously been described as the combination of two components, the high-frequency and low-frequency regions, which correspond to the SEI resistance (R_{SEI}) and charge transfer resistance (R_{CT}), respectively [3-2]. In the obtained plots, a distinct semicircle at high-frequency regions around 100 kHz with a capacitance value of 10^{-7}~10^{-9} Fcm^2 represent the interfacial reaction at the anode/inorganic solid electrolyte [3-11]. The

SEI resistance value of each cycle was calculated using this semicircle. The equivalent circuit used for the fitting of the impedance data was composed of a combination of the electrolyte and the electrode, R_{b+g}, and two *R* // *CPE* (constant phase element) circuits that correspond to the SEI layer and the charge-transfer components, respectively [3-2]. As reported in previous studies for other electrode/electrolyte systems [3-1, 2], it is evident from this figure that the high-frequency semicircles became larger with cycling, indicating an increase in the resistivity of the SEI. Figure 3-5 summarizes the effects of cycling on the SEI resistance values of symmetric cells incorporating the three types of electrolytes and $Li_{4.4}Sn$ electrodes. Prior to cycling, the resistance values of the SEI regions were 48, 41 and 160 Ω for the cells using $Li_{3.5}Ge_{0.5}P_{0.5}S_4$, $Li_{3.35}Ge_{0.65}P_{0.65}S_4$ and $Li_{3.25}Ge_{0.75}P_{0.75}S_4$, respectively. In the initial state, there were no significant differences in the SEI resistivity values due to the cell compositions. However, clear differences in the SEI resistance variations were observed during cycling. The resistance of the $Li_{3.25}Ge_{0.75}P_{0.75}S_4$ cell decreased following the 1st cycle and then slightly increased during subsequent cycles, however the resistance value did not exceed 250 Ω. This behavior was similar to that of the symmetric cell composed of Li–Al/ $Li_{3.25}Ge_{0.25}P_{0.75}S_4$/Al–Li, indicating the formation of a stable SEI layer at the interface. It is worth to note that the resistivity values of these interfaces were comparable to the interface of the oxide films in liquid electrolyte system [3-12], and were extremely lower (by one to three order of magnitude) than those observed for the polymer cells (Li/PEO-$LiCF_3SO_3$/Li cell at 50°C [3-13] and Li/$PEO_{20}LiBF_4$ with 20w/o γ-$LiAlO_2$ /Li cell at 90°C [3-12]). In contrast, a considerable increase is seen in the SEI resistance values of the cells incorporating $Li_{3.35}Ge_{0.65}P_{0.65}S_4$ and $Li_{3.5}Ge_{0.5}P_{0.5}S_4$ throughout the electrochemical cycling. The SEI resistivities of these specimens continuously increased, reaching 458 and 1217Ω after 20 cycles, respectively. These resistance values were at least one order of magnitude greater than the values in the initial state. These results suggest that continuous SEI growth occurred during the cycling until the symmetric cells were essentially destroyed. The SEI resistance values of the cells in the initial state and following the 20th cycle are summarized in Table 3-1, confirming a clear relationship between the solid electrolyte composition and the growth rate of the SEI resistance. Increasing the germanium proportion evidently increased the SEI

resistance rate of increase, indicating that the reduction of germanium could trigger decomposition of the solid electrolyte, thus rendering the SEI layer unsuitable for the necessary reactions in the battery. Because metals can be reduced and/or oxidized more readily than phosphorus, the decomposition of electrolytes containing larger amount of metals is one reason for the increases in both the SEI resistance and thickness. Since the SEI resistance increases during the charge-discharge reaction when employing LGPSx-based electrolytes, the SEI formation and growth might therefore be dependent on the electrochemical stability of the solid electrolyte.

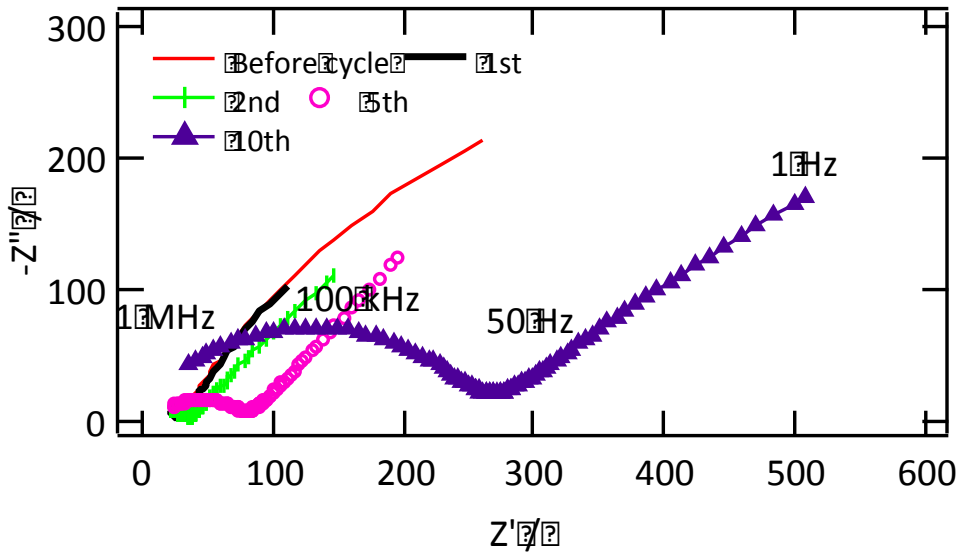

Figure 3-4 Typical examples of the impedance plots measured for the symmetrical cell configuration of $Li_{0.4}Sn$ alloy/ $Li_{3.5}Ge_{0.5}P_{0.5}S_4$/ $Li_{0.4}Sn$ alloy

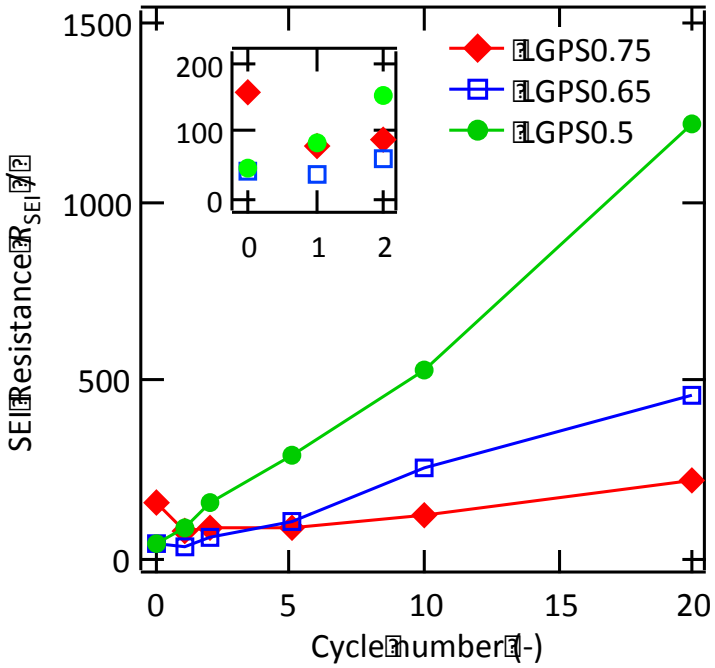

Figure 3-5 Variations in SEI resistance with cycling for cells incorporating sulfide-based solid electrolytes.

Table 3-1 Composition dependence of R_{SEI} prior to cycling and following 20 cycles, and growth rates for the $Li_{4.4}Sn$ / $Li_{4-x}G_{1-x}P_xS_4$ / $Li_{4.4}Sn$ system.

	R_{SEI} prior to cycling	R_{SEI} following 20 cycles	R_{SEI} growth rate	Ge ratio in composition
LGPS0.5	48 Ω	1217 Ω	2535%	5.9%
LGPS0.65	41 Ω	458 Ω	1117%	4.2%
LGPS0.75	160 Ω	218 Ω	136%	3.0%

3.5 Relationship between SEI resistance and electrode composition

However, even though the anode and the solid electrolyte interface play key roles in the battery performance, there is little information available concerning the effects of various combinations of materials and the associated decomposition processes at the negative electrode/electrolyte interface [3-1, 14]. In order to obtain further information concerning the SEI formation process and the resistivity changes during cycling, the effects of electrode composition were examined by varying the Li/M (M = Sn, Si) ratios in the electrodes. The Li/M ratios and redox potentials of the electrodes examined in the present study are summarized in Table 3-1, where the redox potentials of the electrodes are indicated for various lithium contents (y in Li_yM) [3-15, 16]. Figure 3-6 shows the SEI resistance values of cells incorporating Li_yM electrodes with three different $Li_{4-x}Ge_{1-x}P_xS_4$ compositions following 20 cycles. Here the SEI resistances are plotted as functions of the reduction-oxidation (redox) potentials (*vs*. Li/Li^+) of the Li_yM alloys (*V*r). The *V*r potential depends on the lithium proportion in the alloys and therefore the *V*r value of an alloy $Li_{y+z}M$ can vary during the charge-discharge reactions. However, changes in the lithium content with the battery reaction in these symmetrical cells remained within the range defined by $z = \pm 0.003$, demonstrating that the potential changes of the electrodes during the charge-discharge cycles were negligible. Therefore, the *V*r values for the electrodes are plotted using *V*r for the initial y value. In the case of the Li_y-Sn electrode, the SEI resistances decreased with higher *V*r values, indicating that an alloy electrode having a higher *V*r resulted in a stable SEI layer at the electrode/electrolyte interface. This result is in good agreement with the finding that reduction of germanium increases the SEI resistance. Kim *et al*. have reported that GeS_2 exhibits a reduction reaction at potentials below 0.5 V (*vs*. Li/Li^+), and so a *V*r value below 0.5 V was sufficient to obtain the desired SEI resistance [3-17]. These data also confirmed that a higher ratio of germanium in the electrolyte generates increased SEI resistance, especially in the LGPS0.5 system. The SEI resistance in the cell using LGPS0.5 increases over the entire potential range,

though it decreases with higher *V*r values. Although there were slight differences in the absolute values of the SEI resistance between the Li_y-Sn and Li_y-Si electrodes, both electrodes showed almost equivalent trends. The Li_y-Si electrodes with *V*r values below 0.5 V increased the SEI resistivity, while the cell incorporating LGPS0.5 exhibited the highest resistivity of 1294 Ω. These results provide clear evidence that a lower *V*r value enhances the reduction of germanium in $Li_{4-x}Ge_{1-x}P_xS_4$, which in turn triggers the decomposition of the solid electrolyte and increases the impedance of the SEI layer. In addition, the observed threshold potential of approximately 0.5 V also suggests that the reduction of germanium is the dominant factor in the formation and growth of the SEI layer during the battery reaction.

Table 3-1 Redox potentials of the negative electrode materials used in the present study.

Negative materials	Li_y-Sn alloy					Li_y-Si alloy		
y in Li_y-M	0.4	1.0	2.6	3.5	4.4	1.7	2.3	3.3
Redox potential *V* / V [*vs.* Li/Li^+]	0.78	0.69	0.44	0.44	0.43	0.58	0.43	0.4

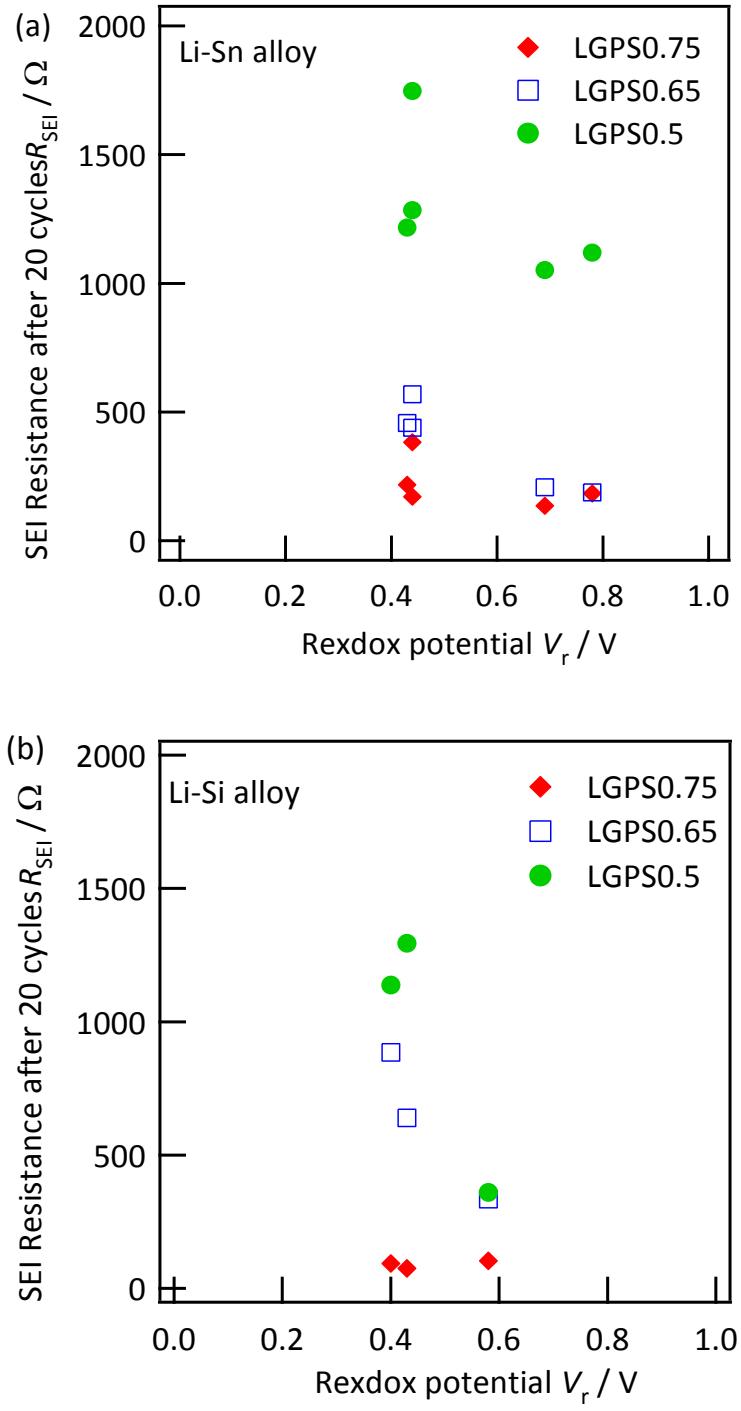

Fig.3-6 Relationship between the SEI resistance of LiSn alloy/SE/LiSn alloy cells (SE: solid electrolyte) following 20 cycles and *V*r, where *V*r is the redox potential of the electrode.

3.6 Observation of the electrode/electrolyte interface

Above mentioned, the increase of SEI resistance has been described to depend on electrolyte composition and redox potential of electrode. In order to control the SEI resistance at electrode/electrolyte interface, it is necessary to understand the SEI layer formation state. The SEI layer formed during the charge-discharge process was characterized by XRD analyses by assessing the surfaces of specimens taken from cells following 20 cycles. To elucidate the relationship between the resistance and the SEI structure, two battery systems were selected: $Li_{3.5}Sn$ alloy/LGPS0.5/$Li_{3.5}Sn$ alloy and $Li_{3.5}Sn$ alloy/LGPS0.75/$Li_{3.5}Sn$ alloy, which had shown SEI resistance values of 1748 and 382 Ω after 20 cycles, respectively. Figure3-7 shows the photographs of the appearance of these electrolyte samples removed the electrode after 20 cycles, respectively. A reaction at the interfacial region was suggested by a change in the color of the electrolyte surface from gray-yellow to dark-gray after 20 cycles. The color of electrolyte surface was found to depend on the increase of SEI resistance with cycling.

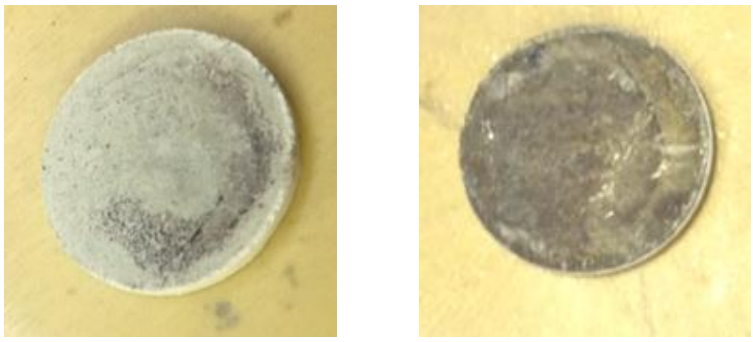

Figure 3-7. The photographs of the appearance of these electrolyte samples after 20^{th} cycles; (a) $Li_{3.5}Sn$ alloy/LGPS0.75 interface (SEI resistance after 20^{th} cycles = 382 Ω) , (b) $Li_{3.5}Sn$ alloy/LGPS0.5 interface (SEI resistance after 20^{th} cycles = 1748 Ω)

Figure 3-8 provides the XRD patterns of the LGPS0.5 and LGPS0.75 specimens in the as-prepared state and following electrochemical cycling. After 20 cycles, the $Li_{3.5}Sn$/LGPS0.5 interface produced clear diffraction peaks originating from an unknown phase, while the diffraction peaks due to the LGPS0.5 had largely disappeared. This specimen corresponds to the highest resistivity in the tested batteries, indicating destruction of the cell during cycling. In the case of the $Li_{3.5}Sn$/LGPS0.75 interface, diffraction peaks from an unknown phase were also observed due to a decomposition product of the electrolyte. However, the intensities of these unknown phase peaks relative to those of the original LGPS0.75 were quite small. This result demonstrates that the LGPS0.75 possesses greater electrochemical stability than the LGPS0.5 due to its lower germanium content. These data show that the lower germanium contents in the solid electrolyte could provide a suitable electrochemical reaction field for battery reaction. *Ex situ* XRD measurements therefore confirmed the decomposition rate of the solid electrolyte and its compositional variation during the battery reactions.

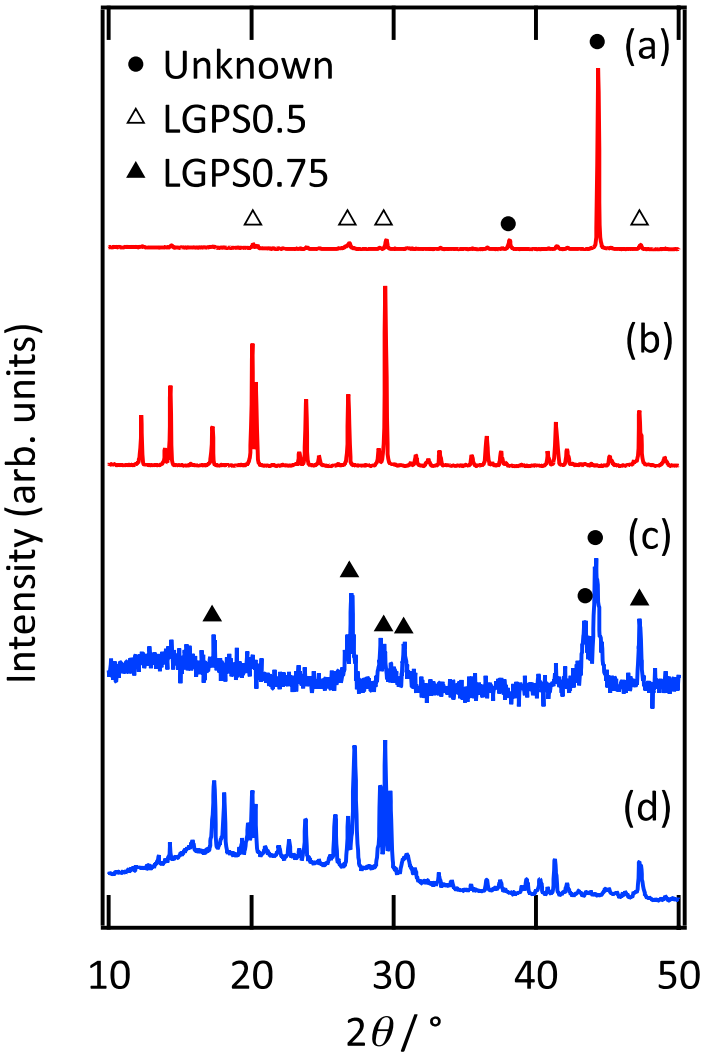

Figure 3-8. XRD patterns of the solid electrolytes: (a) the electrode/electrolyte interface of the $Li_{3.5}Sn$ alloy/LGPS0.5/$Li_{3.5}Sn$ alloy cell after 20 cycles, (b) as-prepared LGPS0.5, (c) the $Li_{3.5}Sn$ alloy/LGPS0.75/$Li_{3.5}Sn$ alloy cell after 20 cycles and (d) as-prepared LGPS0.75.

In order to evaluate changes in the elemental distribution in the electrolyte with cycling, EDX elemental analysis was carried out on a cross-section of the interface of a $Li_{3.5}Sn$ alloy/LGPS0.5/$Li_{3.5}Sn$ alloy cell, both in its initial state and after 20 cycles. Figure 3-9 shows the cross-sectional SEM images of electrolytes removed the electrode (a) initial, (b) after 20 cycles. EDX elemental analyses were carried out within the range of 10 μm from electrode/electrolyte interface. The EDX line analyses were carried out along the red line in the images. Anode electrodes had been removed from the electrolyte before the SEM and EDX measurements. Figure 3-10 shows the changes in the elemental distribution in the electrolyte along the depth direction moving from the electrode/electrolyte interface to the electrolyte bulk. Phosphorus and sulfur levels are seen to increase over a 1 μm range from the surface region with electrochemical cycling while germanium was decreased at the interface, indicating changes in the elemental distribution associated with formation of the SEI. Since Kim *et al.* reported that a reduction of GeS_2 electrode generates Li_2S and Ge-Li alloy [3-17], a hypothesis could be expected that a reduction of the LGPS electrolytes provides three components, the Ge-Li alloy on the anode surface, which might be removed with anode pealing process, Li_2S and Li-P-S materials at the electrolyte surface. These interfacial changes over a 1 μm range and the accompanying electrolyte decomposition might contribute to higher SEI resistance values.

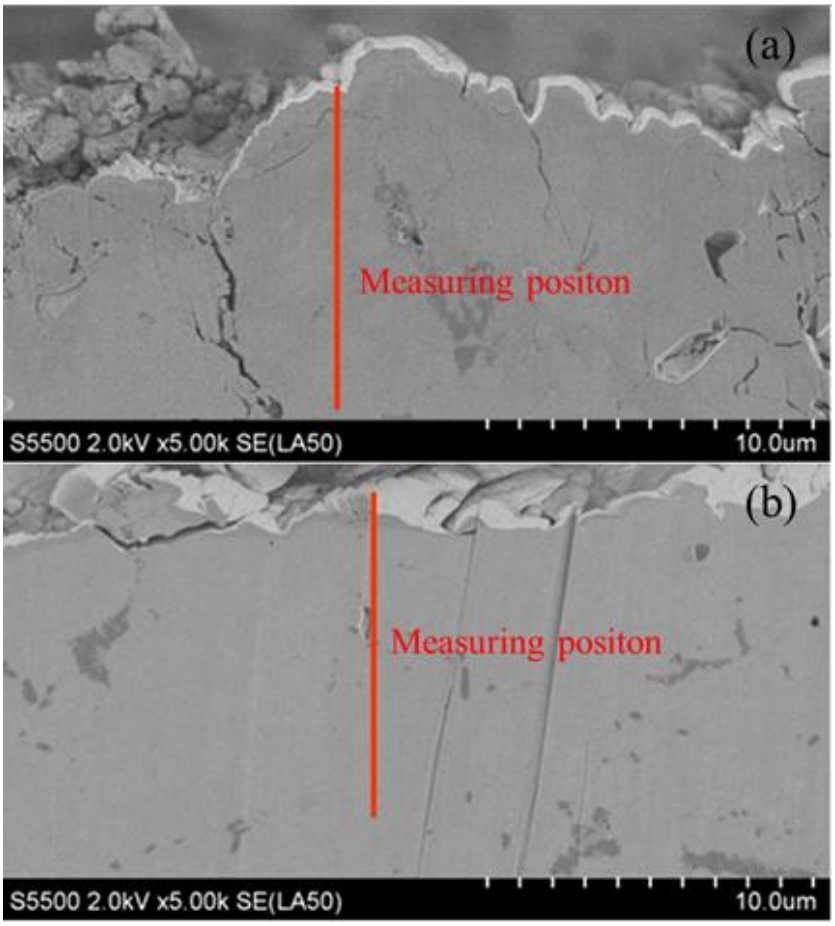

Figure 3-9 SEM image of the cross-sectional electrolyte sample of $Li_{3.5}Sn$ alloy/ LGPS0.5/$Li_{3.5}Sn$ alloy cell, (a) before cycling and (b) after 20 cycles.

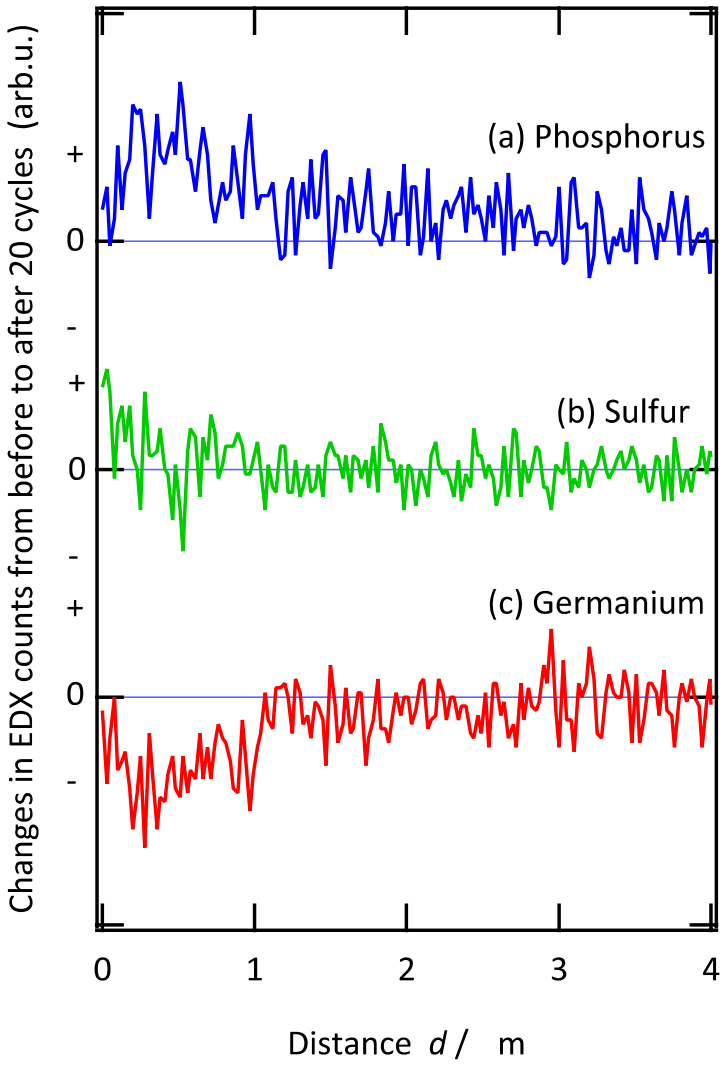

Figure 3-10 Changes in the element distribution along the depth direction for a cross-section following 20 cycles by EDX elemental analysis for a $Li_{3.5}Sn$ alloy/ LGPS0.5/$Li_{3.5}Sn$ alloy cell.

3.7 Effect of SEI composition

To assess the SEI composition effects on resistance, charge-discharge measurements were carried out with artificial additives at the $Li_{0.4}Sn$/LGPS0.5 interface. Three materials were selected as additives: Li_2S (Nihon Kagaku Kogyo), GeS_2 (Kojundo Chemical Laboratory, 99.9% > purity) and P_2S_5 (Aldrich, 99.9% > purity). These additives all represent raw ingredients for the synthesis of LGPSx, and thus could be expected to be present at the interface after decomposition reactions due to the SEI formation. The process by which these new cells were fabricated was essentially the same as that used to produce the earlier, non-additive cells. The desired additive in powder form was added in the amount of approximately 1 mg to the electrolyte pellet, distributed over one side, after which the pellet was pressed at 184 MPa and a $Li_{0.4}Sn$ alloy electrode was subsequently pressed onto the additive material layer. The other side of the specimen was constructed in the same manner so as to maintain symmetry. Figure 3-11 shows the variations of the SEI resistances of these symmetric cells incorporating additives upon cycling. The initial SEI resistances of the cells with additives were comparable to that of the non-additive cell, indicating that the additives did not affect the initial impedance at the interface remarkably; non-additive = 28 Ω, and with-additives P_2S_5 = 97 Ω, Li_2S = 70 Ω, GeS_2 = 17 Ω.

.The SEI resistances of all cells were increased with cycling, and it is noteworthy that there was a clear difference in the SEI resistance growth rates. The SEI resistances were increased to 2009 and 1511 Ω when incorporating the additives P_2S_5 and Li_2S, respectively. Conversely, the cell with GeS_2 as an additive showed comparable resistance to that of the non-additive cell; non-additive = 1119 Ω and with GeS_2 = 1291 Ω. Following 20 cycles, the SEI resistance of the cell to which P_2S_5 has been added at the electrode/electrolyte interface was the highest of the four cells. This result indicated that P_2S_5 additive reacted with Li_2S and/or Li-ion at the interface, and this reaction could contribute to further Li-P-S compounds formation. Thus, the presence of Li-P-S phases at the electrode/electrolyte interface generated by the decomposition of the LGPSx solid electrolyte could be expected to increase the SEI resistance. In addition, P_2S_5 might increase the growth rate of the Li-P-S phases by the

reaction with Li_2S and enhance continuous decomposition reaction at the interface.

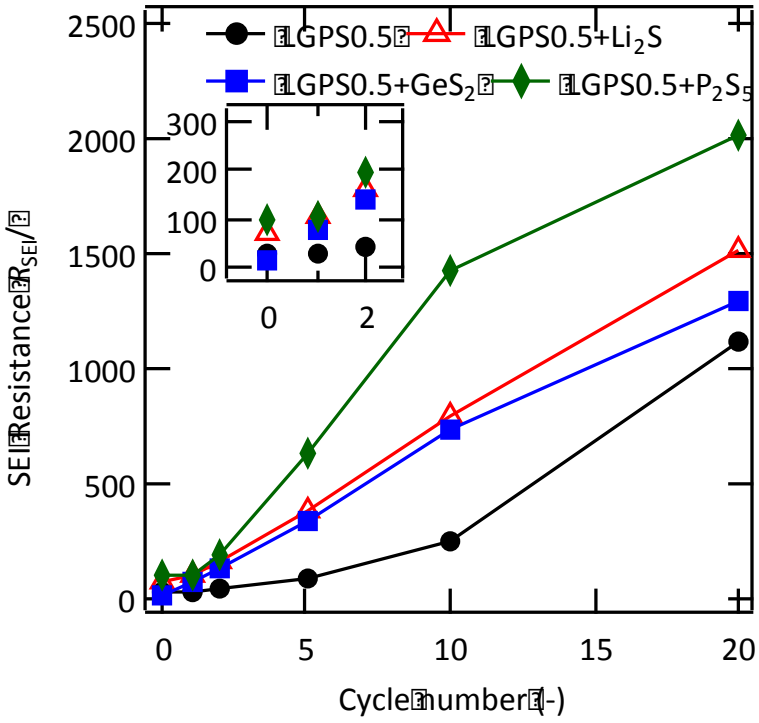

Figure 3-11 Cycling dependence of the SEI resistance for cells with added Li_2S, GeS_2 and P_2S_5 at the $Li_{0.4}Sn$ alloy/LGPS0.5 interface.

3.8 Conclusion

The stability of the electrode and electrolyte interface was studied in all-solid-state batteries with sulfide-based solid electrolytes.

The electrolyte composition was found to influence the charge-discharge characteristics of the all solid-state batteries with $Li_{4-x}Ge_{1-x}P_xS_4$ electrolyte. The relation between the electrolyte composition and cycle performance on the SEI resistance values of symmetric cells incorporating the three types of electrolytes and Li.Sn alloy electrodes was studied. Solid electrolyte of the composition with smaller *x* value in $Li_{4-x}Ge_{1-x}P_xS_4$ contributes to thicker SEI formation due to the instability of the Ge in the LGPS structure during battery reactions.

On the other hand, the electrode composition for Li_y-M (M=Sn, Si) alloy was found to influence the charge-discharge characteristics of the all solid-state batteries with $Li_{4-x}Ge_{1-x}P_xS_4$ electrolyte. The relation between the electrode composition and cycle performance on the cycling on the SEI resistance values of symmetric cells incorporating sulfide based solid electrolyte and Li-M (M=Sn, Si) electrodes was studied. Smaller interfacial resistances were observed for cells using Li-M (M = Sn, Si) alloy electrodes with higher redox potentials (*vs.* Li/Li^+).

The SEI layer was found to increase the SEI resistance and become thicker during cycling. The structure of the SEI layer is amorphous and L-P-S compounds generated by electrolyte decomposition at the interface electrode/electrolyte could be responsible for the observed increase the observed increase in resistance. The presence of L-P-S compounds in SEI layer could be expected to increase the SEI resistance. In addition, P_2S_5 might increase the growth rate of the Li-P-S phases by the reaction with Li_2S and enhance continuous decomposition reaction at the interface.

References

[3-1] T. Kobayashi, A. Yamada and R. Kanno, *Electrochim. Acta* **53** (2008) (15), p. 5045.

[3-2] R. Kanno, M. Murayama, T. Inada, T. Kobayashi, K. Sakamoto, N. Sonoyama, A. Yamada and S. Kondo, *Electrochem. Solid-State Lett.* **7** (2004) (12), p. A455.

[3-3] R. Kanno, and M. Murayama, *J. Electrochem. Soc.*, **148**, 742 (2001).

[3-4] R. Kanno, T. Hata, Y. Kawamoto, and M. Irie, *Solid State Ionics,* **130**, 97 (2000).

[3-5] M. Murayama, R. Kanno, M. Irie, S. Ito, T. Hata, N. Sonoyama, and Y. Kawamoto, *J. Solid State Chem.*, **168**, 140 (2002).

[3-6] N. Kamaya, K. Honma, Y. Yamakawa, M. Hirayama, R. Kanno, M. Yonemura, T. Kamiyama, Y. Kato, S. Hama, K. Kawamoto and A. Mitsui, Nat Mater **10** (2011) (9), p. 682.

[3-7] N. Ohta, K. Takada, I. Sakaguchi, L. Zhang, R. Ma, K. Fukuda, M. Osada and T. Sasaki, *electrochemistry Communications*, 9 (2007), 1486-1490.

[3-8] C. Wang, A. John Appleby and F.E. Little, *J. Power Sources* **93** (2001) (1–2), p. 174.

[3-9] R.Z. Hu, L. Zhang, X. Liu, M.Q. Zeng and M. Zhu, *Electrochem. Commun.* **10** (2008) (7), p. 1109.

[3-10] T. Sakai, *Electrochemistry* **71** (2003) (8), p. 722.

[3-11] K. Takada, M. Tansho, I. Yanase, T. Inada, A. Kajiyama, M. Kouguchi, S. Kondo and M. Watanabe, *Solid State Ionics* **139** (2001) (3–4), p. 241.

[3-12] R. Zanoni, F. Decker, C. Coluzza, F. Artuso, N. Cimino, G. Di, Santo, and E. Masetti, *Surf. Interface Anal.*, **33**, 815 (2002).

[3-13] R. N. Mason, M. Smith, T. Andrews, and D. Teeters, *Solid State Ionics*, **118**, 129 (1999).

[3-14] R. Kanno, M. Murayama, T. Inada, T. Kobayashi, K. Sakamoto, N. Sonoyama, A. Yamada and S. Kondo, *Electrochem*. *Solid-State Lett*. **7** (2004) (12), p. A455.

[3-15] K. Hirai, T. Ichitsubo, T. Uda, A. Miyazaki, S. Yagi and E. Matsubara, *Acta Mater*. **56** (2008) (7), p. 1539.

[3-16] W.J. Weydanz, M. Wohlfahrt-Mehrens and R.A. Huggins, *J*. *Power Sources* **81–82** (1999) (0), p. 237.

[3-17] Y. Kim, H. Hwang, K. Lawler, S.W. Martin and J. Cho, *Electrochim Acta* 53 (2008) (15), p. 5058.

CHAPTER 4

Development of novel lithium ion conducting oxy-sulfides in Li-P-S-O system: its structure and electrochemical properties

4.1 Introduction

Sulfides lithium ion conductors have been attracted much attention due to its high ionic conductive properties. Especially, $Li_{10}GeP_2S_{12}$ (LGPS) shows extremely high conductive value over 10^{-2} S cm^{-1} at room temperature, which is comparable to the counterpart of the organic liquid electrolyte [4-1]. However, it was revealed that a germanium in this material systems trigger a serious resistance increase of a solid electrolyte interphase (SEI) layer due to an electrochemical reduction during the battery operation. This finding indicates that the Li-Ge-P-S system materials cannot be used in practical all solid-state battery with a use of low voltage negative electrode such as Li-M alloy, carbon and lithium metal while these materials could increase the energy density of the batteries. In addition, intrinsic poor chemical stability of sulfides is also to be considered for its application to battery products. Recently, wide variety of the LGPS family and its solid solutions have been developed by substitution of the Ge by Si or Sn [4-2, 3, 4]. These LGPS-type materials show high ionic conductivity over 10^{-3} S cm^{-1}, and are isostructural to the original LGPS with a space group of $P4_2/mmc$. However,

metal free LGPS family has not been discovered to date, and decrease of sulfur content in the structure by oxygen substitution is strongly expected to achieve higher electrochemical/chemical stability of the material. In this study, novel lithium ion conductive oxy-sulfides with the LGPS structure were searched in a ternary diagram of Li_2S-P_2S_5-P_2O_5 system and its structure and electrochemical properties were investigated. The SEI resistance of Li-P-S-O systems in symmetrical cell was also evaluated via charge-discharge and ac-impedance measurements.

4.2 Synthesis and characterization of Li-P-S-O solid electrolyte

The ternary diagram of Li_2S-P_2S_5-P_2O_5 system is shown in Figure 4-1, illustrating searched composition in this study with blue triangles. A tie line between Li_3PS_4 and Li_3PO_4 was reported by Takada *et al.* [4-5] while LGPS type structure formation was not reported. For materials search, a parent composition of $Li_{3+5x}P_{1-x}S_4$ where $x = 0.07$ was selected because this composition shows highest ionic conductivity in the Li_2S-P_2S_5 system of thio-LISICON family [4-6]. The $Li_{3.35}P_{0.93}S_4$ can be described as $Li_{10.05}P_{2.79}S_{12}$, which is expected to be a new $Li_{10}GeP_2S_{12}$ family based on the previous report of Si and Sn systems [4-7]. Partially substitution of sulfur by oxygen was carried out for the $Li_{3.35}P_{0.93}S_4$ along with various z values in a composition of $Li_{3.35}P_{0.93}S_{4-z}O_z$.

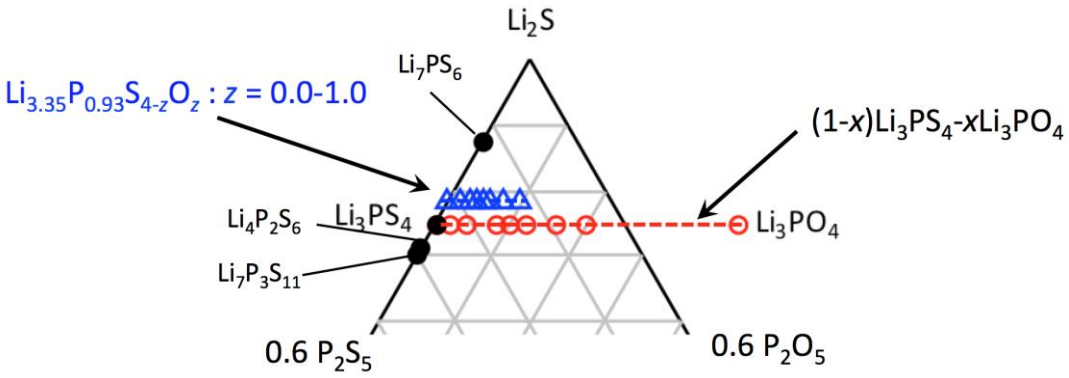

Fig.4-1 Ternary diagram of Li_2S-P_2S_5-P_2O_5 system and searched composition in this study. Representative reported materials are also illustrated.

The $Li_{3.35}P_{0.93}S_{4-z}O_z$ solid electrolytes were synthesized by solid-state reaction with quenching method using Li_2S (Kojyundo Chemical Laboratory Co., Ltd., 99% purity), P_2S_5 (Aldrich, 99% purity) and P_2O_5 (Kojyundo Chemical Laboratory Co., Ltd., 99.99% purity) as starting materials. They were weighed in appropriate molar ratios in an Ar-filled glove box, and ground by a vibrating mill (CMT, Tl-100) for 30 min. The ground powders were pressed into pellets and then sealed in a carbon-coated quartz tube at 10 Pa. The pellets were heated to 973 K with a heating rate of 2 K min^{-1}, after 1 h the pellets were cooled down using water bath. X-ray diffraction data of the samples were collected by X-ray diffractometer (Rigaku SmartLab) with CuKα radiation with each 0.03° step width over the 2θ range from 10° to 35°. Synchrotron X-ray diffraction measurement was conducted using the BL02B2 beamline at SPring-8 for structural analysis at room temperature. The X-rays were monochromated using a Si(111) double crystal system and the X-ray with a wavelength of 0.6 Å was selected. Synchrotron X-ray Rietveld analysis was performed to determine the structural parameters using Rietan-FP. Phase determination was carried out by the XRD measurements as shown in Figure 4-2. Small z range from 0 to 0.3, clear diffraction patterns of the LGPS type are not observed while distinct peaks from γ-Li_3PS_4 are clearly seen around 20 and 23°. In addition, another impurity phase of Li_7PS_6 was confirmed from the diffraction peak at 30°. The intensity of γ-Li_3PS_4 peaks decreases

with z value and the LGPS type diffraction liens appear more pronounced. Although the Li_7PS_6 peaks are still confirmed, LGPS type patterns are observed as a main phase in the z range from 0.4 to 0.6. Further increase of z over 0.8 provides additional unknown peaks around 22°. These results indicates that solid solution of the LGPS type oxy-sulfide exists around $z = 0.5$ in $Li_{3.35}P_{0.93}S_{4-z}O_z$. To characterize the LGPS type oxy-sulfide, the $Li_{3.35}P_{0.93}S_{3.5}O_{0.5}$ ($z = 0.5$) was subjected to further investigation.

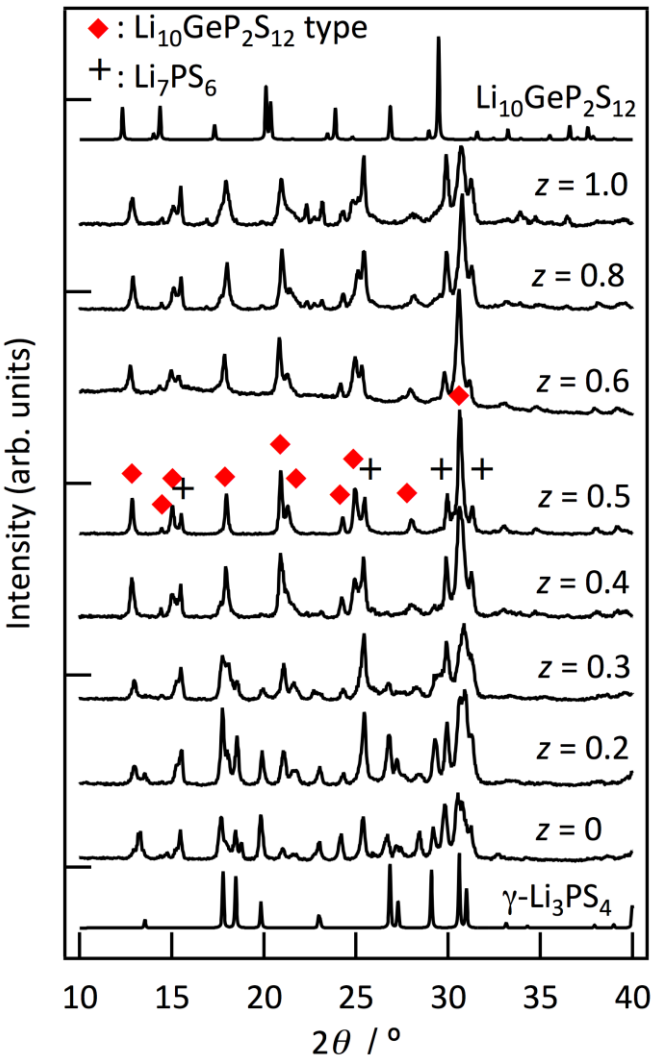

Fig.4-2 XRD patterns of $Li_{3.35}P_{0.93}S_{4-z}O_z$ in $0 \leq z \leq 3.0$. XRD patterns of γ-Li_3PS_4 and $Li_{10}GeP_2S_{12}$ from ICSD #180318 and #248307, respectively, are also illustrated.

Rietveld refinement using synchrotron XRD was carried out for the $Li_{3.35}P_{0.93}S_{3.5}O_{0.5}$ (z = 0.5), and analysis results are summarized in Figure 4-3 and table 4-1. Space group $P4_2/nmc$ was selected as structural model for the refinement with four different lithium sites [4]. All the parameters of lithium were fixed along with the previous reports using neutron diffraction data. The wavelength of the incident beam was calibrated using a NIST SRM Ceria 640b CeO_2 standard and was fixed at 0.59866 Å. A good fitting result was obtained using the LGPS-type and Li_7PS_6 impurity phases. Contracted lattice parameters of $Li_{3.35}P_{0.93}S_{3.5}O_{0.5}$ (z = 0.5) compared to the original LGPS were confirmed due to smaller ions substitutions; P^{5+} (0.17 Å) < Ge^{4+} (0.39 Å), O^{2-} (1.4 Å) < S^{2-} (1.84 Å). Lower ionic conductivity of this material (9.1 x 10^{-5} S cm^{-1}) could be attributed to this contracted lattice. Cation substitution at P(2) site with a small amount of vacancy and anion substitution at S(1) site were respectively confirmed. These results evidently revealed the LGPS type novel oxy-sulfide material formation. In addition, preferred substitution sites were confirmed.

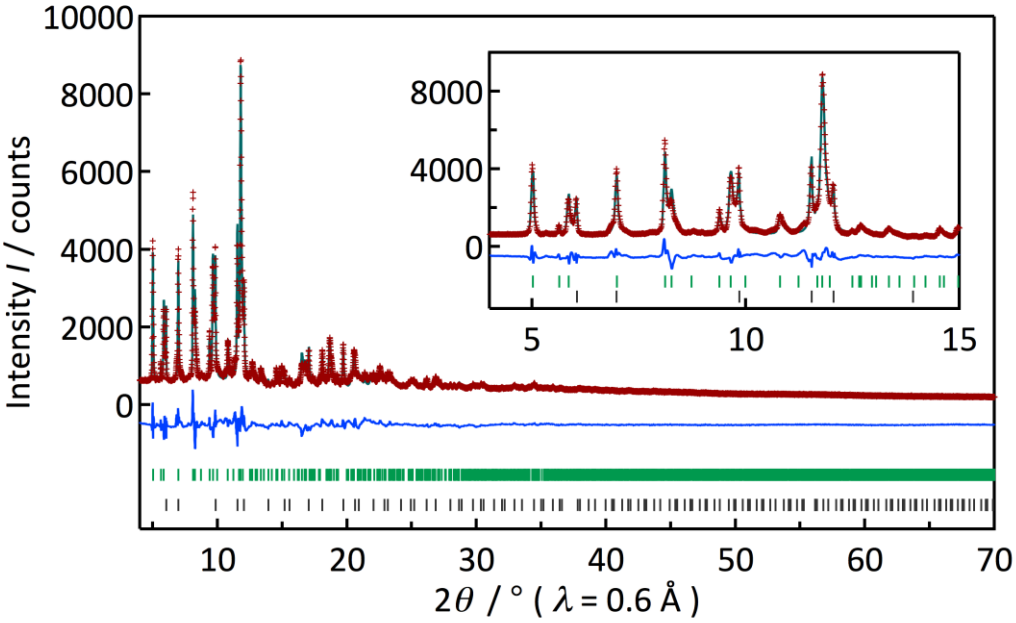

Fig.4-3 Synchrotron X-ray Rietveld refinement patterns for $Li_{3.35}P_{0.93}S_{3.5}O_{0.5}$ (z = 0.5). Observed data points are indicated by cross marks (+) and solid lines overlaying the data were obtained via Rietveld refinement analysis. Vertical markers below the patterns indicate positions of possible Bragg reflections of space group $P4_2/nmc$ for $Li_{3.35}P_{0.93}S_{3.5}O_{0.5}$ (green) and impurity Li_7PS_6 (black) phases. Differences between observed and calculated intensities are plotted below the data on the same scale.

Table 4-1. Structural parameters obtained from Rietveld refinement analysis on synchrotron XRD data of $Li_{3.35}P_{0.93}S_{3.5}O_{0.5}$ using $P4_2/nmc$ space group.

Atom	Site	g	x	y	z	B (Å^2)
P(1)	4*d*	1.0	0.0	0.5	0.6835(5)	1.09(7)
P(2)	2*b*	0.79(12)	0.0	0.0	0.5	= *B*[P(1)]
S(1)	8*g*	0.671(8)	0.0	0.1730(4)	0.4173(3)	2.55(9)
O(1)	8*g*	= 1-*g*[S(1)]	0.0	= *y*[S(1)]	= *z*[S(1)]	= *B*[S(1)]
S(2)	8*g*	1.0	0.0	0.2940(4)	0.0974(3)	= *B*[S(1)]
S(3)	8*g*	1.0	0.0	0.7023(4)	0.7804(2)	= *B*[S(1)]
Li(1)	16*h*	0.38	0.26	0.27	0.19	5.0
Li(2)	4*d*	1.0	0.0	0.5	0.95	3.0
Li(3)	8*f*	0.83	0.24	0.24	0.0	5.0
Li(4)	4*c*	0.84	0.0	0.0	0.26	5.0

Unit cell: tetragonal $P4_2/nmc$ (137); a = 8.3702(3) Å, c = 12.3023(6) Å, V = 861.92(6) Å^3; R_{wp} = 7.034, R_p = 5.094, R_b = 2.115, R_R = 16.232, R_e = 4.472, goodness of fit S = R_{wp}/R_e = 1.57; phase: Li_7PS_6 (*ca.* 21.1 mass%).

4.3 Electrochemical properties of Li-P-S-O solid electrolyte

Ionic conductivity of the $Li_{3.35}P_{0.93}S_{3.5}O_{0.5}$ and its temperature dependence were evaluated ac-impedance measurements. Obtained Nyquist plots and Arrhenius plots are shown in Figure 4-4. One semicircle and a spike were observed for all temperature tests and the capacitance value of the semicircle was about 10^{-10} F. Therefore, separation of components for bulk and grain boundary could not be achieved. The conductivity value was calculated using the semicircle as total resistance. A conductivity of 9.1 x 10^{-5} S cm^{-1} was confirmed at 25°C, indicating a lattice contracted effects of the LGPS structure. The activation energy of 36.6 kJ mol^{-1} was 50% larger than those of other LGPS family [4-1, 2, 3, 4], indicating the conduction mechanism change of the materials and/or impurity effects of this compounds.

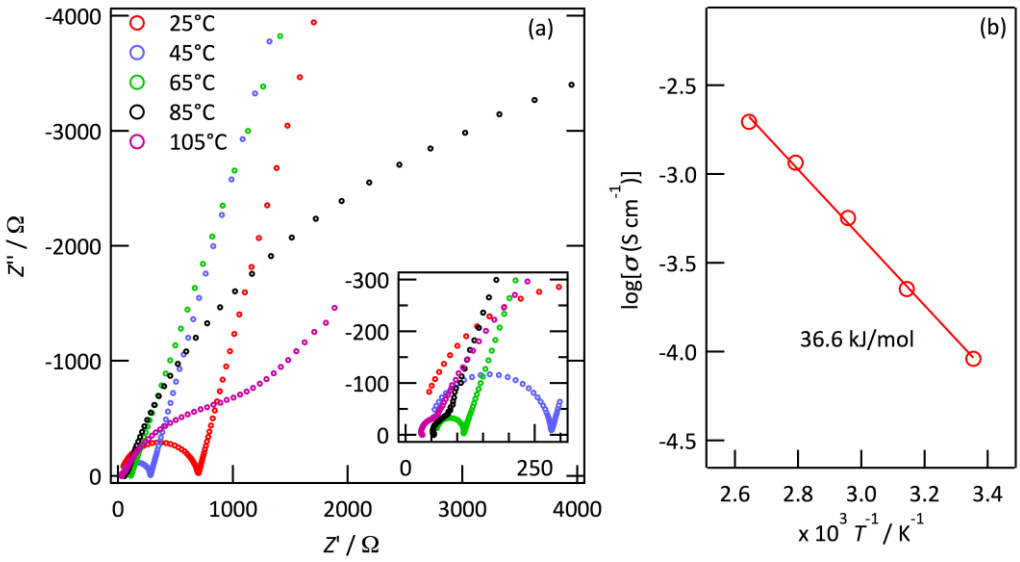

Fig.4-4 Nyquist plots at various temperatures for $Li_{3.35}P_{0.93}S_{4-z}O_z$ (z = 0.5) (a) and Arrhenius plots using obtained impedance data. The magnified Nyquist plots are also included in (a).

CV curve using asymmetric cell with a configuration of Li/solid-electrolyte/Au is illustrate in Figure 4-5. Except for the currents near 0 V with lithium deposition and dissolution, no significant current peak was observed. The $Li_{3.35}P_{0.93}S_{3.5}O_{0.5}$ is electrochemically stable in voltage range from -0.5 to 5 V (*vs.* Li/Li^+). Smaller value of the current compared to that of the LGPS could be due to low ionic conductivity of this material. The excellent electrochemical stability of the oxy-sulfide is revealed and application to solid-state battery with wide voltage range can be expected.

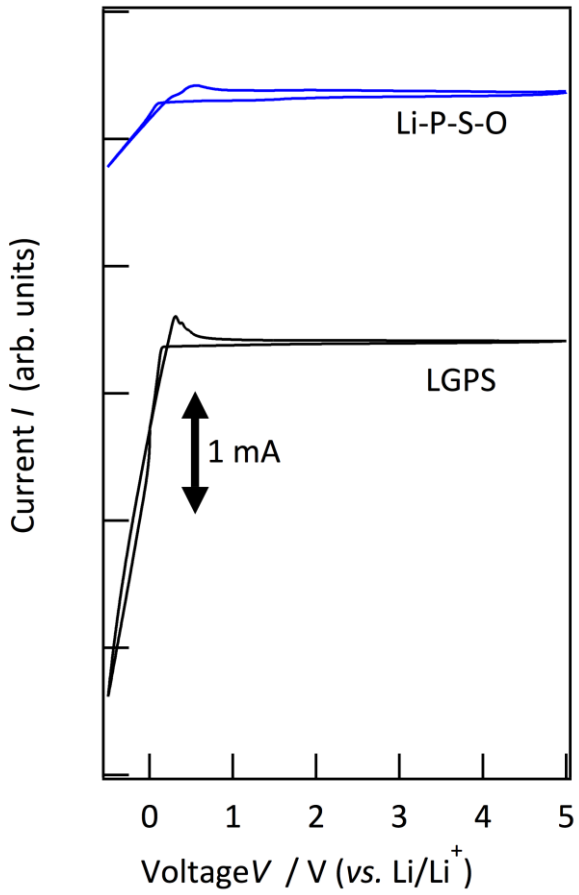

Fig.4-4 Nyquist plots at various temperatures for $Li_{3.35}P_{0.93}S_{4-z}O_z$ (z = 0.5) (a) and Arrhenius plots using obtained impedance data. The magnified Nyquist plots are also included in (a).

4.4 Effects of the solid electrolyte composition to the SEI resistance

Charge-discharge tests were carried out with the symmetric cells ($Li_{0.4}Sn$/solid electrolyte/$Li_{0.4}Sn$) by applying a constant current of 1.38 mA cm^{-2} for 20 min, following which the same amount of current was applied after switching the current direction. Redox voltage of the $Li_{0.4}Sn$ alloy is about 0.8 V (*vs*. Li/Li^+). After each cycle of the charge-discharge process, the ac impedance of the cell was measured. All the electrochemical experiments were carried out at room temperature (25 ºC). The SEI resistance was calculated using a semicircle at high-frequency region in the

obtained impedance plots [4-8, 9]. The SEI resistances and its cycle dependence are shown in Figure 4-4. At the initial cycle, LGPS systems showed lower resistance compared to the LPSO systems. This could be due to the intrinsic higher ionic conductivity of the LGPS system. However, repeating the cycles increased the SEI resistance of the LGPS system while the LPSO system showed an opposite trend. As revealed in chapter 3, the Ge content in the structure strongly affects to the SEI resistance, more Ge rich LGPS050 showed the highest resistivity over 1000 Ω. On the other hand, the LPSO system showed significant decrease in the resistance from 600-1000 Ω to 30-110 Ω. Germanium free $Li_{3.35}P_{0.93}S_{4-z}O_z$ (z = 0.0) showed significant resistance suppression. Furthermore, $Li_{3.35}P_{0.93}S_{4-z}O_z$ (z = 0.4) showed lowest resistance, indicating that the oxygen substitution could contribute to a formation of the well-contacted SEI layer during the charge-discharge process. The SEI layer formed at oxy-sulfide could provide better interface, which suppresses further electrolyte decomposition and contributes to better ionic lithium ion diffusion and charge transfer reaction. Since larger amount of impurity phases in contained as prepared state, the $Li_{3.35}P_{0.93}S_{4-z}O_z$ (z = 0.8) showed slight larger resistance. As a result, these electrochemical evaluations demonstrated that the novel LGPS type oxy-sulfides without metal elements (Li-P-S-O) could be a good candidate as solid-electrolyte for all-solid-state lithium battery using low redox voltage anode materials, and contribute to increase in energy density of the batteries.

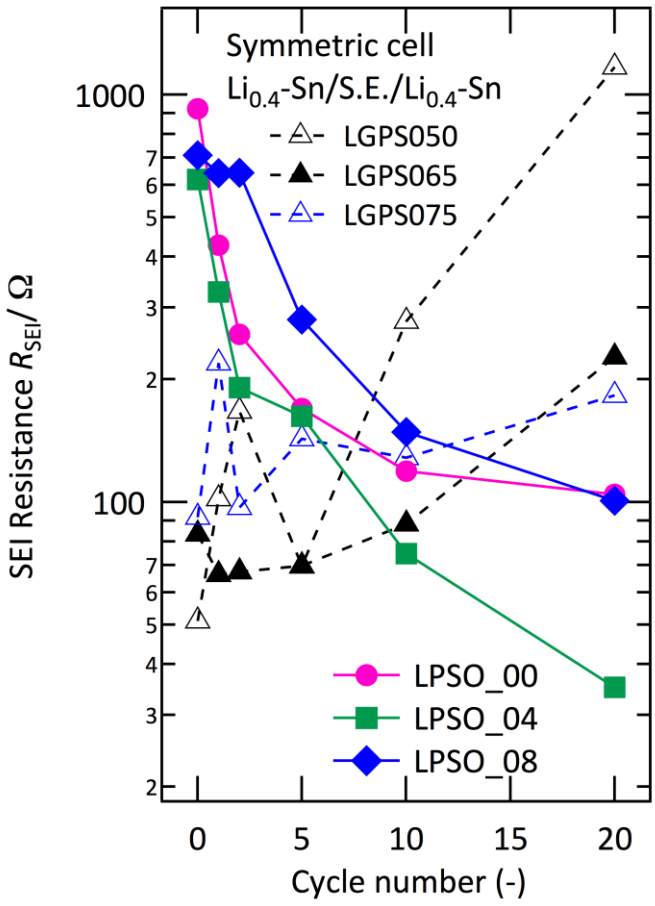

Fig.4-4 Cycling dependence of the SEI resistance for cells $Li_{0.4}Sn$/S.E interface. Results of LGPSx ($Li_{4-x}Ge_{1-x}P_xS_4$) system and LiPSOz ($Li_{3.35}P_{0.93}S_{4-z}O_z$) system are plotted as a function cycle number.

4.5 Conclusion

The novel lithium ion conducting oxy-sulfides of Li-P-S-O system with LGPS type structure were developed, and its structure and electrochemical properties were evaluated. Dominant LGPS type phase formation in the composition of $Li_{3.35}P_{0.93}S_{4-z}O_z$ with z from 0.4 to 0.6 was confirmed. Structural analysis for $Li_{3.35}P_{0.93}S_{3.5}O_{0.5}$ (z = 0.5) revealed that the novel oxy-sulfide is isostructural to the original LGPS and preferred P and S/O substitution in the structure occurred in the crystal structure. Lower ionic conductivity of the $Li_{3.35}P_{0.93}S_{3.5}O_{0.5}$ (z = 0.5): 9.1 x 10^{-5} S cm^{-1}, and larger activation energy: 36.6 kJ mol^{-1} compared to the counterparts of the original LGPS could be due to the lattice contraction and conduction mechanism changes/impurity formation. Electrochemical stability in a voltage region from -0.5 to 5.0 V was confirmed cyclic voltammetry. SEI resistivity and its cycle dependence evaluation demonstrated that the novel LGPS type oxy-sulfides without metal elements (Li-P-S-O) provides lower resistivity and well-contacted SEI layer during the charge-discharge process. These results indicate the novel oxy-sulfides could be a good candidate as solid-electrolyte for all-solid-state lithium battery using low redox voltage anode materials, and contribute to increase in energy density of the batteries.

References

[4-1] N. Kamaya, K. Homma, Y. Yamakawa, M. Hirayama, R. Kanno, M. Yonemura, T. Kamiyama, Y. Kato, S. Hama, K. Kawamoto and A. Mitsui, *Nat Mater*, **10**, (2011) p. 682.

[4-2] S. Hori, K. Suzuki, M. Hirayama, Y. Kato, T. Saito, M. Yonemura and R. Kanno, *Faraday Discuss*., **176**, (2014) p. 83.

[4-3] Y. Kato, R. Saito, M. Sakano, A. Mitsui, M. Hirayama and R. Kanno, *J*. *Power Sources*, **271**, (2014) p.60.

[4-4] O. Kwon, M. Hirayama, K. Suzuki, Y. Kato, T. Saito, M. Yonemura, T. Kamiyama and R. Kanno, *Journal of Materials Chemistry A*, **3**, (2015) p. 438.

[4-5] K. Takada, M. Osada, N. Ohta, T. Inada, A. Kajiyama, H. Sasaki, S. Kondo, M. Watanabe and T. Sasaki, *Solid State Ionics*, **176**, (2005) p. 2355.

[4-6] M. Murayama, N. Sonoyama, A. Yamada and R. Kanno, *Solid State Ionics*, **170**, (2004) p. 173.

[4-7] S. Hori, K. Suzuki, M. Hirayama, Y. Kato, T. Saitoo, M. Yonemura and R. Kanno, *Faraday Discuss*. (2014).

[4-8] T. Kobayashi, A. Yamada and R. Kanno, *Electrochim*. *Acta*, **53**, (2008) p. 5045.

[4-9] R. Kanno, M. Murayama, T. Inada, T. Kobayashi, K. Sakamoto, N. Sonoyama, A. Yamada and S. Kondo, *Electrochem*. *Solid-State Lett*., **7**, (2004) p. A455.

CHAPTER 5

Summary

For the development of all-solid-state lithium batteries, comprehensive understanding of electrode/electrolyte interface is required, and ideal interfacial structure construction based on the reaction mechanism is important. Although the interface plays key role for the battery reactions, interfacial reactions in all sold state batteries including solid electrolyte interphase (SEI) layer formation are still under investigation. In the present study, the reactions at electrode/electrolyte interface of all solid-state batteries were studied for combinations of sulfide-based solid electrolytes and various compositions of alloy as negative electrodes.

This thesis contains of two main studies to elucidate the interfacial reaction and SEI layer behavior in the solid-state battery.

In chapter 3, various compositional sulfides lithium conductors; $Li_{4-x}Ge_{1-x}P_xS_4$, thio-LISICON and Li_y-M (M=Sn, Si) alloys were applied in the battery and electrochemical evaluations. Redox potential effects of the anode revealed that the lower redox voltage electrodes provided higher resistive SEI layer. In addition, compositional dependence of the solid electrolyte confirmed larger proportion of Ge in the electrolyte conducted to larges SEI resistance values. As a result, electrochemical reduction of Ge in the electrolyte and its continuous degradation generated increasing of the SEI resistance while low Ge content electrolytes provided electrochemically stable SEI layer which could work for reversible charge discharge reaction. Finally, it was revealed that the low conductive Li-P-S compounds at the interface could contributed to the resistance increasing.

In chapter 4, novel lithium ion conducting oxy-sulfides were developed, which has no metal element and partially substituted sulfur atom by oxygen in the structure. The new materials exist in a ternary diagram of Li_2S-P_2S_5-P_2O_5 system and have isostructure to

$Li_{10}GeP_2S_{12}$ with superionic conductivity. The materials form a solid solution in a limited range in the composition of $Li_{3.35}P_{0.93}S_{4-z}O_z$ with z from 0.4 to 0.6. Structure analysis for $Li_{3.35}P_{0.93}S_{3.5}O_{0.5}$ (z = 0.5) revealed that the novel oxy-sulfide is isostructural to the original LGPS and preferred P/defect formation and S/O substitution occurred at the specific sites in the crystal structure. Lower ionic conductivity of the $Li_{3.35}P_{0.93}S_{3.5}O_{0.5}$ (z = 0.5): 9.1 x 10^{-5} S cm^{-1}, and larger activation energy: 36.6 kJ mol^{-1} compared to the counterparts of the original LGPS could be due to the lattice contraction and conduction mechanism changes/impurity formation. SEI resistivity and its cycle dependence evaluation demonstrated that the novel Li-P-S-O provides lower resistivity and well-contacted SEI layer during the charge-discharge process. These results indicate the novel oxy-sulfides could be a good candidate as solid-electrolyte for all-solid-state lithium battery using low redox voltage anode materials, and contribute to increase in energy density of the batteries.

Detailed analysis of the interface layer in the solid-state battery revealed degradation mechanisms, and showed solid electrolyte material design indication especially for the composition. Controlling the SEI layer composition and its growth rate by the solid-electrolyte materials could be a new method to develop the all-solid-state batteries with higher energy density and long cycle stability.

Acknowledgement

The author would like to express his appreciation to Professor Ryoji Kanno of Tokyo Institute of Technology for his continuous guidance and valuable discussions on this thesis.

The author greatly wishes to thank Associate Professor Masaaki Hirayama, and Assistant Professor Kota Suzuki of Tokyo Institute of Technology for their encouragements.

The author wishes to thank Professor Takeo Osaka, Professor Jiro Nakamura, and Associate Professor Fusao Kitamura of Tokyo Institute of Technology for their review of this thesis.

The author wishes to make grateful acknowledgement to the members of Kanno-Hirayama's Laboratory for continuous encouragements and helpful discussions.

Finally, the author would like to express his sincere gratitude to his family for their support, understanding, and encouragement.

December 2015

Masamitsu SAKUMA